2017•2018
Faculteit Industriële ingenieurswetenschappen
master in de industriële wetenschappen: elektronica-ICT

Masterthesis

Model-based optimization of electrodes for lithium-ion batteries

PROMOTOR :
Prof. dr. ir. Jan GENOE

COPROMOTOR :
Prof. dr. Mohammadhosein SAFARI

Ferhat Avci, Devlin Voets

Scriptie ingediend tot het behalen van de graad van master in de industriële wetenschappen: elektronica-ICT

Gezamenlijke opleiding UHasselt en KU Leuven

2017 • 2018

Faculteit Industriële ingenieurswetenschappen

master in de industriële wetenschappen: elektronica-ICT

Masterthesis

Model-based optimization of electrodes for lithium-ion batteries

PROMOTOR :

Prof. dr. ir. Jan GENOE

COPROMOTOR :

Prof. dr. Mohammadhosein SAFARI

Ferhat Avci, Devlin Voets

Scriptie ingediend tot het behalen van de graad van master in de industriële wetenschappen: elektronica-ICT

Words of gratitude

This master's thesis is the report from our research period as master's student in industrial engineering electronics – ICT, an education at the University of Hasselt and the Catholic University of Leuven. During this period we had the opportunity to do research at the Materials & Applications Engineering group of the IMO-IMOMEC research centrum (University of Hasselt).

First, we would like to thank Prof. Dr. Ir. Momo Safari and Prof. Dr. Ir. Jan Genoe for giving us the opportunity to work on this thesis and for their guidance, patience, and support during this period. Secondly, we would like to thank Ing. Hamid Hamed and Ing. Saeed Yari, their commitment, ideas, and support made this work possible. Finally, we would also like to thank our friends and family for their support and understanding during these hard and stressful times.

The elaboration of this master thesis has been a tremendously educational experience and had a strong impact on us in the development as an industrial engineer.

Ferhat Avci and Devlin Voets

Table of contents

List of tables

List of figures

List of symbols and subscripts

a	specific interfacial area, m^2/m^3
$\boldsymbol{c}$	concentration of electrolyte, mol/dm^3
$\boldsymbol{c_i}$	concentration of species *i*, mol/dm^3
$\boldsymbol{c_s}$	concentration of lithium in solid phase, mol/dm^3
$\boldsymbol{c_T}$	total concentration from all species
$\boldsymbol{D}, \boldsymbol{D_s}$	diffusion coefficient of electrolyte and of lithium in the solid matrix, cm^2/s
$\boldsymbol{D_{ij}}$	interaction value between species *i* and *j*, cm^2/s
$\boldsymbol{f_A}$	activity coefficient of salt
$\boldsymbol{f_\pm}$	mean molar activity coefficient of the salt
F	Faraday's constant, 96487 C/mol
$\boldsymbol{i}$	current density, mA/cm^2
$\boldsymbol{i_{0,x}}$	exchange current density, mA/cm^2
$\boldsymbol{i_{1,x}}$	electronic current
$\boldsymbol{i_{2,x}}$	ionic current
$\boldsymbol{I}$	total current density, mA/cm^2
$\boldsymbol{j_n}$	pore-wall flux across interface, mol/m^2
$\boldsymbol{\kappa}$	reaction rate constant
L	thickness, m
r	radial distance in a particle of the active material, m
R	gas constant, 8,3143 J/(mol*K)
$\boldsymbol{R_e}$	Electronical resistance, ohm
$\boldsymbol{R_s}$	radius of a solid particle, m
t	time, s
$\boldsymbol{t_i^0}$	transference number of species *i* with respect to the solvent
T	temperature, K
U	open-circuit potential, V
x	distance between current collector and electrode
y	stoichiometric coefficient of lithium in active material
$\boldsymbol{\alpha}$	charge transfer coefficient
$\boldsymbol{\delta_i}$	thickness of material *i*, m
$\boldsymbol{\varepsilon}$	porosity
$\boldsymbol{\eta}$	overpotential, V
$\boldsymbol{\rho_i}$	density of material *i*, g/cm^3
$\boldsymbol{\sigma}$	ionic conductivity (solid matrix), S/cm
$\boldsymbol{\mu_i}$	electrochemical potential of species *i*, J/mol
$\boldsymbol{\varphi}$	electrical potential, V

-	negative electrode
+	positive electrode
a	anode
c	cathode
e	electrolyte
eff	effective value of transport property
f	filler
p	polymer
s	separator
1	solid matrix
2	solution phase

Abstract

The battery division of EMAP department is researching electrochemical cells and energy storage which includes the optimization of cathode materials for lithium-ion batteries. The cathode is a crucial element that determines to a large extent the capacity and power of a lithium-ion battery.

Investigating the sensitivity of the battery performance to the different design parameters (i.e., electrode thickness, electrode composition, solid-state diffusion coefficient, ionic conductivity, electronic conductivity, and porosity) is essential for optimizing the performance of the cell. The sensitivity analysis is done using Doyle's Dualfoil program, an efficient simulation tool for lithium-ion batteries.

In this project, four different cathode materials are studied (i.e., LCO, NMC, LMO, and LFP). A reference cell is defined that fulfill the practical capacity of each material. Each of the design parameters is changed separately, simulated and the effects on the cells performance is observed and discussed. Some parameters have an intuitive impact on the cell performance while others demonstrate a complex trend which is only possible to be revealed with the aid of simulations. The energy and power of the cell are shown to be highly sensitive to parameters such as thickness, porosity, and the solid-state diffusion coefficient of lithium.

Abstract

De batterijafdeling van de EMAP-afdeling onderzoekt elektrochemische cellen en energieopslag, waaronder ook het onderzoek naar kathodematerialen valt. Het kathodemateriaal is bepalend voor de capaciteit en het vermogen van de lithium-ion batterijen.

Het onderzoek naar de gevoeligheid van de batterij prestaties voor de verschillende ontwerpparameters (elektrodedikte, elektrodesamenstelling, *solid-state* diffusiecoëfficiënt, ionische geleidbaarheid, elektronische geleidbaarheid en porositeit van de kathode) is essentieel voor het optimaliseren van de prestaties van een cel. De gevoeligheidsanalyse wordt uitgevoerd met het Dualfoil-programma van Doyle, een efficiënt simulatie hulpmiddel voor lithium-ion batterijen.

In dit project worden vier verschillende kathodematerialen bestudeerd (LCO, NMC, LMO en LFP). Er is een referentie cel gedefinieerd die de praktische capaciteit van elk materiaal behaald. Elk van de ontwerpparameters wordt afzonderlijk gewijzigd, gesimuleerd en de effecten op de prestaties van de cellen worden waargenomen en besproken. Sommige parameters hebben een intuïtieve invloed op de cel prestaties, terwijl andere een complexe trend vertonen die alleen kan worden onthuld met behulp van simulaties. Er wordt aangetoond dat de energie en het vermogen van de cel zeer gevoelig zijn voor parameters zoals dikte, porositeit en de *solid-state* diffusiecoëfficiënt van lithium.

1 Introduction

1.1 Background

IMEC (Interuniversity Micro-Electronics center) is the biggest independent research center of Europe in the fields of microelectronics, nanotechnology and digital technology. IMEC was founded in 1984 as a non-profit organization as result of a program started by the Flemish Government to strengthen the microelectronics industry in Flanders. IMEC has its headquarter in Leuven, it is also present in different countries such as The Netherlands, Taiwan, China, India, United States, and Japan [1].

The Institute for Materials Research (IMO) is a research center of Hasselt University, it has a collaboration with IMOMEC (Institute for Materials Research in Micro-Electronics) a department from IMEC. The main activities of IMO-IMOMEC consist of research in wide band gap materials, organic synthesis, organic materials for electronic applications, precursors for nanomaterial's, biosensors, nanophysics and electrical, physical and chemical characterization [2].

Engineering Materials & Applications (EMAP) is a research group within IMO-IMEC linked to the faculty of industrial Engineering. EMAP's research covers three major domains: biomedical device engineering, energy systems engineering, and manufacturing of functional Materials [3].

1.2 Problem statement

Lithium-ion batteries (LIBs) contain an anode, a cathode, an electrolyte, and a separator. Upon initial cell assembly, the cathode material is the source of lithium and the anode is the sink. The electrolyte ensures the ionic transport between the two electrodes. A separator is a porous membrane that is placed between the anode and cathode, permeable to ionic flow but preventing electronic contact of the electrodes. On discharge, electrons leave the anode via an external circuit where they do useful work before entering the cathode. Thus, the electrodes must allow for the flow of both lithium ions and electrons. That is, they must be both good ionic and electronic conductors. Most of the electrochemically-active materials used as cathode and anode in the LIBs are not good electronic conductors, so it is necessary to include in the electrode formulation some electronically conductive additives such as carbon black. To physically hold the electrode contents together, a polymeric binder is used. Thus, the electrodes in LIBs are complex porous composites soaked in a liquid electrolyte [4].

In order to design LIBs with an optimal performance one must understand how various parameters affect their operation and therefore mathematical modeling and simulation are very helpful. The cathode is one of the important components in a LIB that is decisive for the capacity and power of the LIBs. The goal of this thesis is to investigate the sensitivity of the battery performance to the different design parameters (i.e., electrode thickness, electrode composition, solid-state diffusion coefficient, ionic conductivity, electronic conductivity, and porosity of the cathode) for the main cathode materials in common use in the state-of-the-art LIBs. Table 1 shows some of the properties of these materials.

*Table 1: Four materials of three different crystal structure that are being researched, * practical capacity*

Materials	**Structure**	**Range voltage (V)**	**Specific capacity (mAh/g)**	**Specific energy (mWh/g)**	**Average potential w.r.t. Li/Li+ (V)**
LMO	Spinel	4.5 - 3	148 (100 – 120*)	410 - 492	4.1
NMC	Layered	4.2 - 2.5	278 (160 – 170*)	610 - 650	3.8
LCO	Layered	4.85 - 3.6	273 (140*)	546	3.9
LFP	Olivine	3.6 - 2	170 (150 – 170*)	518 - 587	3.45

1.3 Objectives

Here, the main objective is to perform a systematic investigation of the influence of the main adjustable design parameters on the performance of a LIB with the aid of Physics-based modeling and simulation. Since the cathode has the most crucial role for the capacity of a LIB and in order to simplify the analyses, a half-cell setup is used where a lithium foil is used as the anode electrode instead of a composite anode. Lithium manganese oxide ($\mathrm{LiMn_2O_4}$ or LMO), lithium nickel manganese cobalt oxide ($\mathrm{LiNiMnCoO_2}$ or NMC), lithium cobalt oxide ($\mathrm{LiCoO_2}$ or LCO), and lithium iron phosphate ($\mathrm{LiFePO_4}$ or LFP) are the cathode materials considered in this study and the following design parameters are studied in the sensitivity analyses:

- Solid-state Li diffusion coefficient in cathode material
- Electronic conductivity of the cathode
- Ionic conductivity of the electrolyte
- Cathode thickness
- Cathode composition
- Porosity of the cathode

1.4 Approach and methods

The battery division of EMAP department uses COMSOL Multiphysics as their simulation program, it is as the name says a multi-physics solver. This software is very user friendly but at the expense of quite long computation time which is not pleasant for optimization and sensitivity analyses purposes. There exist however an efficient program for simulating lithium-ion batteries in Fortran language: Doyle's Dualfoil program [5]. Here, Dualfoil is used as the source code and further elaborated in order to create a user-friendly program for fast and efficient simulation of LIBs.

2 Literature study of the battery

Emerge of portable devices throughout the decades led to the development of rechargeable batteries. The ever growing interest to replace conventional cars with electric vehicles (EVs) and plug in hybrid electric vehicle (PHEVs), has emphasized the need for better rechargeable batteries that have low weight, high specific energy, high rate capability, low cost, and most importantly a high level of safety. Among the rechargeable batteries, LIBs can deliver more capacity in comparison to other batteries shown in the Ragone plot in Figure 1 and they are currently the state-of-the-art and widely used in portable devices, EVs and PHEVs [6] [7].

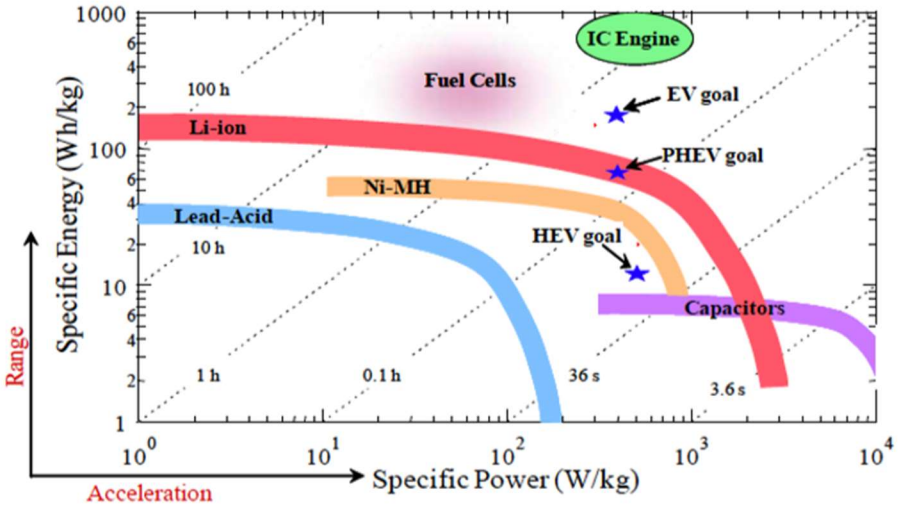

Figure 1: Ragone plot of various electrochemical energy storage and conversion devices, obtained from [8]

A battery is an energy storage system used for converting electrical energy that is produced at a certain time (e.g., from renewable sources such as wind or solar energy) into electrochemical energy. The stored electrochemical energy can be converted back into electrical energy and used at a later time. The conversion from chemical to electrical energy and vice versa is a result of redox reactions inside the electrodes. There is a difference between chemical and electrochemical redox reactions. A chemical redox reaction is when the reduction and oxidation are taking place in the same region. Unlike 'chemical' redox, in 'electrochemical' redox reactions, oxidation and reduction occur at different electrodes, i.e., cathode and anode. During discharge, oxidation and reduction reactions take place at anode and cathode, respectively. Batteries that can be recharged and are designed to have multiple charges and discharges are called secondary batteries. In such batteries, during charge, oxidation and reduction reactions at cathode and anode, respectively, will prepare the battery for a new discharge. On the other hand, there are primary batteries capable of converting their chemical energy to electrical energy only one time, also known as disposable batteries. The term 'battery' or better-called 'battery packs' are commonly used when multiple electrochemical cells are connected together to make a desired power and voltage output [7] [8].

2.1 Lithium-ion cell

The Li-ion half-cell shown in Figure 2, consists of two current collectors, a porous cathode, a lithium foil anode, a separator and the electrolyte. These major components are detailed in this chapter.

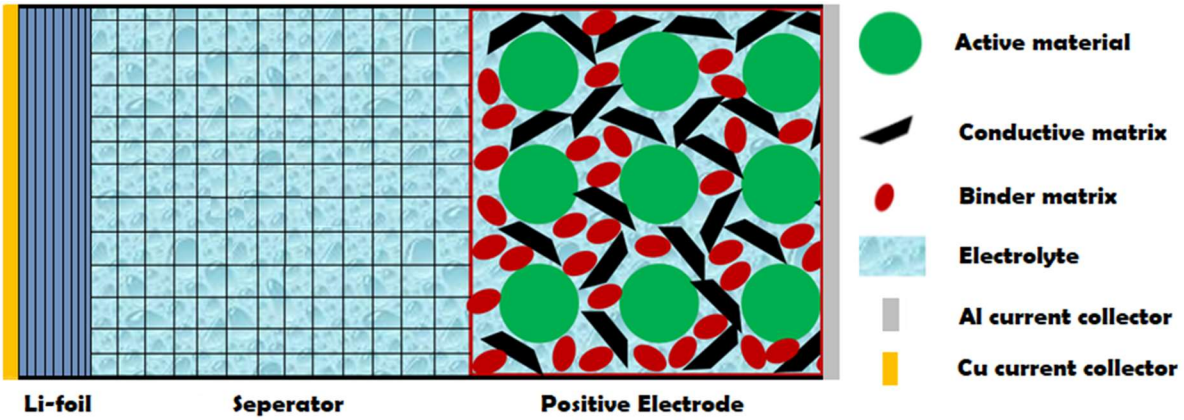

Figure 2: Representation of the Lithium half-cell, reproduced from [9]

The lithium cell that has essentially two electrodes: the positive porous electrode and the negative porous electrode also known as full-cell lithium cells. The cell portrayed in Figure 2 is a half-cell, the negative porous electrode is replaced with a lithium foil. The lithium foil can be seen as a pool of lithium clustered together from which lithium ions are generated during discharge and are plated back on the Li foil during charge. Such a half-cell design was originally commercialized as 'Lithium battery' before LIBs but were withdrawn shortly from the market due to the formation of Li dendrites during charge and safety issues. Accordingly, in LIBs, carbon-based porous electrodes replaced the lithium foil.

The porous electrode consists of different materials such as active material. The active material acts as a host structure for lithium ions that can reversibly enter and leave it during charge or discharge. In addition to that, the porous electrode contains binder and conductive additives. The conductive additive ensures the electronic contact between the active materials and the current collector. The binder is a polymeric glue that holds everything together in place, this material is chemically inert and non-conductive for electrons and ions. The open porosity of the porous electrode is filled with an electrolyte containing positive Li-ions and their counterpart negative ions. The reaction rates on the pore walls and its distribution depend on the microstructure (e.g., porosity and tortuosity), conductivity of the matrix, conductivity of the electrolyte, and on the properties of the active-material [10].

Both the anode and the cathode are casted on the current collectors namely copper for the anode and aluminum for the cathode. The selection of the current collectors depends on two main criteria: electronic conductivity and electrochemically stability when in contact with the cell components at low and high potentials. The working potential for common anodes is in the range of 0.5V to 2.5V vs. Li. Copper has an electrochemical activity at an approximate potential of 2.7 V vs. Li, therefore Cu is selected as the current collector for anodes with carbon-based active materials. In cathodes of which the working potential is ~3V to 4.7V vs. Li, aluminum is an appropriate current collector (Al becomes electrochemically active around 4.7V vs. Li) [11].

The separator separates both electrodes so there is no electrons transport internally possible otherwise, this will result in a short circuit.

2.2 Operation of a lithium-ion cell

The battery is fully charged when the active materials at cathode are fully de-lithiated (free of lithium) whereas the porous anode or the lithium foil, is in a fully lithiated state (full of lithium). There is an electrochemical-potential difference between the two electrodes which forces the instantaneous flow of electrons and lithium ions from the anode towards the cathode during cell discharge as seen in Figure 3. When enough time given after charging, the electrolyte will uniformly diffuse across the cell [12].

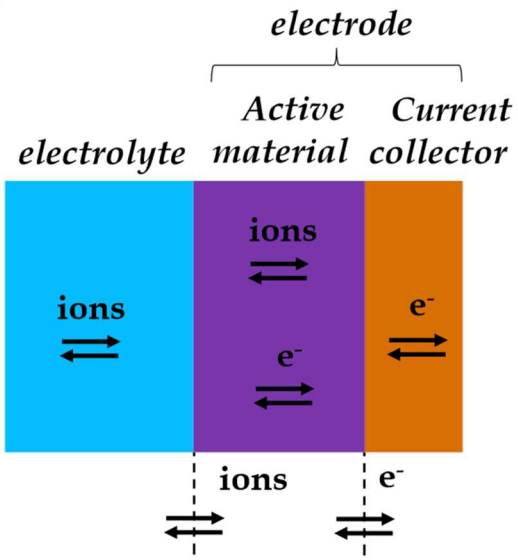

Figure 3: Movement of ions and electrons between interfaces, obtained from [9]

During discharge, when the cell is externally closed, with a load, the electrons will move towards the cathode. Driven by a difference in the electrochemical potential of electrons between the two electrodes, oxidation will happen at the anode and reduction at the cathode during cell discharge. Electrons travel via the external circuit whereas the Li ions released from the active material host enter the electrolyte and move towards the cathode. The release of lithium ions near the anode and their uptake at the cathode side creates a concentration gradient inside the electrolyte; the Li ions will diffuse from the higher concentration towards the lower concentration. The transport rate of lithium ions in the electrolyte can limit the discharge power of the cell. When the load is high enough, the release and uptake of lithium at the electrodes cannot last long since a very large concentration gradient will soon develop across the cell and leads to a premature end of discharge. The discharge ends when the cut-off voltage (~2-3V) of the cell is reached or the cathode material is fully lithiated [12].

2.3 Anode active materials

Lithium foil in LIBs is replaced with a porous electrode, due to the instability of the solid electrolyte interphase and irregular deposition at the surface of lithium. Common replacement for lithium foil is a graphite anode. The crystal structure consists of layered graphene planes, see Figure 4, with a good mechanical stability, lithium transport, and electrical conductivity. Between the graphene planes, Li-ions (de)inserted without causing a significant volume change. The potential for de(lithiation) is quite low which is an advantage when compared to other insertion-based anode candidates[8].

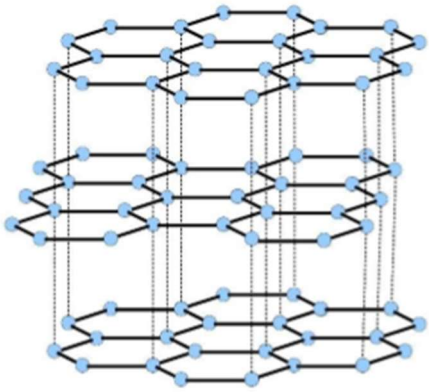

Figure 4: The crystal structure of graphite, obtained from [11]

Graphite anodes are low cost, abundant, have high Lithium diffusivity and electrical conductivity. Compared to lithium foil, graphite has an average insertion potential which is 0.1V higher and its specific capacity is around 372 mAh/g which is significantly lower than 3862.5 mAh/g of lithium foil. The irreversible side reactions at the interface of graphite and liquid electrolyte are a major source of capacity loss and aging. Such side reactions are more pronounced during the first few charge/ discharge cycles, but can continue over the course of battery life. For instance, the solid electrolyte interphase layer (SEI) can deteriorate due to the mechanical stress during charge/discharge, and the consequent reformation of SEI leads to a continuous loss of capacity. Alternative replacements for lithium foils are alloys with lithium. Lithium alloys do have a very high specific charge compared to graphite but due to short life cycle and large volume changes, they are not yet competitive with graphite [8] [13].

2.4 Cathode active materials

An important component of the LIBs is the active material used in the cathode. Cathode is often the most expensive component of a LIB. The conventional cathode materials for LIBs can be categorized in three major groups according to their crystal structures: 2D layered, 3D spinel, and 1D olivine, shown in Figure 5. The dimension of the structures has effect on the diffusion of the Li-ions into the material [12] [14].

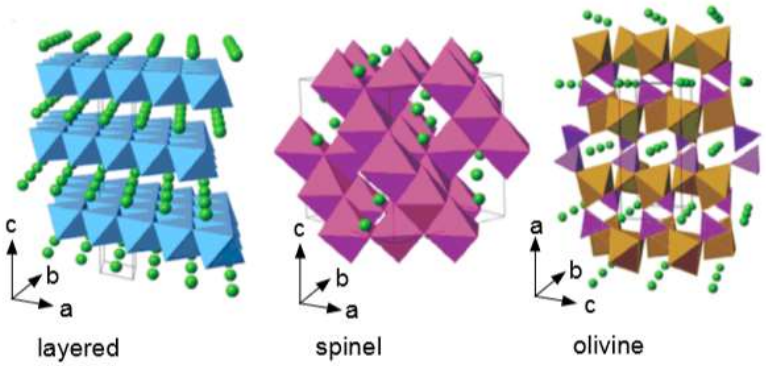

Figure 5: Crystal structure in major Li-insertion host cathodes: layered, spinel, and olivine, obtained from [13]

Every crystal structure has its own attribute, the layered structure is used for high energy systems, the spinel and olivine structures are preferred for high power LIBs. The specific capacity of different cathode materials is listed in Table 2. Besides capacity, other parameters such as chemical stability, rate capability, cost and safety, are of prime importance for a cathode material [13].

*Table 2: ''Electrochemical characteristics of three main groups of insertion cathode materials in lithium-ion batteries'' [13], * practical capacity*

Framework	**Compound**	**Specific capacity (mAh/g)**	**Average potential (V vs. Li^0/Li)**
Layered	LCO	272 (140*)	4.2
	NMC333	272 (200*)	4.0
Spinel	LMO	148 (120*)	4.1
	LMN	148 (120*)	4.7
Olivine	LFP	170 (160*)	3.45
	LFMP	170 (160*)	3.4/4.1

The layered LCO ($LiCoO_2$) is the first commercialized successful cathode material by SONY and introduced by Goodenough. This material is still used today, it has a high specific capacity of 274 mAh/g, main drawback is release of oxygen when the material is heated beyond a certain temperature, resulting in a reaction causing the LIB going in flames [14].

The spinel LMO ($Li_yMn_2O_4$) is one of the promising cathodes in terms of cost, abundance, and non-toxicity, yet suffers from shortcomings such as irreversible capacity loss during multiple cycles and loss of capacity at elevated temperature [8] [14].

The layered NMC ($Li_yNi_xMn_xCo_{1-2x}O_2$) structure has earned great attention as replacement of LCO in LIBs, thanks to its better stability during cycling even at elevated temperatures, higher reversible capacity and better thermal stability at charged state. Combination of nickel, manganese, and cobalt in this cathode leads to higher charge/discharge capacity, lower material cost and the absence of the monoclinic distortion at the state of charge of 50% compared to LCO [8] [14].

The Olivine LFP ($\mathrm{LiFePO_4}$) has an approximate operating voltage of 3.45 V vs. Li and a theoretical capacity of 170 mAh/g, but in reality, this can vary between 150-160 mAh/g. The open-circuit-voltage (OCV) profile is flat which indicates a two-phase mechanism for (de)insertion of lithium. LFP has a low electronic conductivity which is smaller than 10^{-9} S/m and having a low solid-state diffusion coefficient for lithium ions around 10^{-14} m²/s. However, it has a long cycle life, is inexpensive, abundant, and non-toxic [11] [13].

Table 3 shows a summary of the advantages and disadvantages of each material described above.

Table 3: ''Relative merits of selected commercial Li-ion battery cathodes'' obtained from [15] and [14]

Advantages	Disadvantages
LMO ($\mathbf{Li_yMn_2O_4}$ and variants)	
Low cost	
Excellent high rate performance	Mn solubility issue, affecting cycle life
High operating voltage	Low capacity
No resource limitation	
Moderate safety (oxygen release)	
NMC ($\mathbf{Li_yNi_{1/3}Mn_{1/3}Co_{1/3}O_2}$ and variants)	
High capacity	High cost of Ni and Co
High operating voltage	Potential resource limitations
Slow reaction with electrolytes	
Moderate safety (oxygen release)	
LFP ($\mathbf{LiFePO_4}$)	
Moderately low cost	Low operating voltage
Excellent high rate performance	Low capacity, especially for substituted variants
No resource limitations	
Very slow reaction with electrolyte	
Excellent safety (no oxygen release)	
LCO ($\mathbf{LiCoO_2}$)	
High theoretical specific capacity	High cost of Co
High theoretical volumetric capacity	Low thermal stability
Low self-discharge	Fast capacity fade at high current rates
High discharge voltage	Release of oxygen
Good cycling performance	

2.5 Electrolyte

The electrolyte is an important part of the LIBs not only because it is a medium that allows the transport of ions, but also because it is an easier component to modify in order to optimize the LIBs for high current and power applications. Therefore the choice of the electrolyte is critical. Most importantly the electrolyte needs to have a high ionic conductivity because it has a great impact on the specific power of the cell, further it needs a good electronic insulation. In addition to that, the electrolyte needs to be stable when in contact with strong oxidizing/reducing surface of the electrodes: side reactions can occur at the electrodes/electrolyte interface and electrolyte can decompose [11] [16].

Electrolytes are essentially salts dissociated into anions and cations with the help of a solvent. The non-aqueous organic solvents are used in conventional LIBs. Typical organic solvents are: propylene carbonate (PC), Ethylene carbonate (EC) and a mixture of Dimethyl carbonate (DMC) with EC. PC has an extensive range of temperature, but the disadvantage is the capacity fading due to the reduction of PC on the lithium surface. EC has a high dielectric constant but a high melting point. The mix of DMC/EC provides benefits such as lower melting temperature and viscosity of the mixture. Today solvents are commonly mixtures of EC with a linear carbonate. The fundamental flaw of organic solvents is the high toxicity and flammability [8].

The salt must have the following properties: non-toxicity, high solubility in the solvent and the anions stability against oxidative decomposition at the cathode and inertness to electrolyte solvents and cell components. Salts such as $LiClO_4$, $LiAsF_6$, $LiBF_4$, and $LiPF_6$ have become the most used salt as a result of well-balanced properties. EC is one of the solvents used with $LiPF_6$ [11].

The driving forces for the movement of ions inside the electrolyte is the presence of a non-zero gradient of the electrochemical potential for ions across the cell. It is a common practice, however, to interpret the transport of ions by migration and diffusion phenomena. First, migration is the movement of charged species in the electrical field. Secondly, there is diffusion which is the movement of the species due to the difference/gradient in the concentration of ions. [18].

A comprehensive description of the transport properties of a given electrolyte requires determination of $(n-1)/2$ transport properties, where n is the number of independent species present in the electrolyte, according to Onsager reciprocal relations. In an electrolyte composed of $LiPF_6$ in a single solvent, n=3 and therefore three independent transport properties do exist. The three transport properties obtained from the Onsager reciprocal relation are the conductivity κ, salt diffusion coefficient $\mathfrak{D}_{eff}$ and the transference number t_+^0. The concentration gradient inside the electrolyte is mainly dictated by these three parameters in a binary electrolyte [16].

3 Modelling

The one-dimensional macroscopic model of a lithium-ion cell has been developed by Newman et al and further coded in Fortran by Doyle. The 1D representation of a LIB is shown in Figure 6, where the electrochemical cell is divided in three main sections: starting from the left $0 < x < L_{-}$ the anode (negative electrode), $L_{-} < x < L_{sep}$ the separator and $L_{sep} < x < L_{+}$ the cathode (positive electrode). A sub model for the active materials is used to explain the state of lithiation or concentration of lithium, in the radial direction (*r)*, in the solid phase [17].

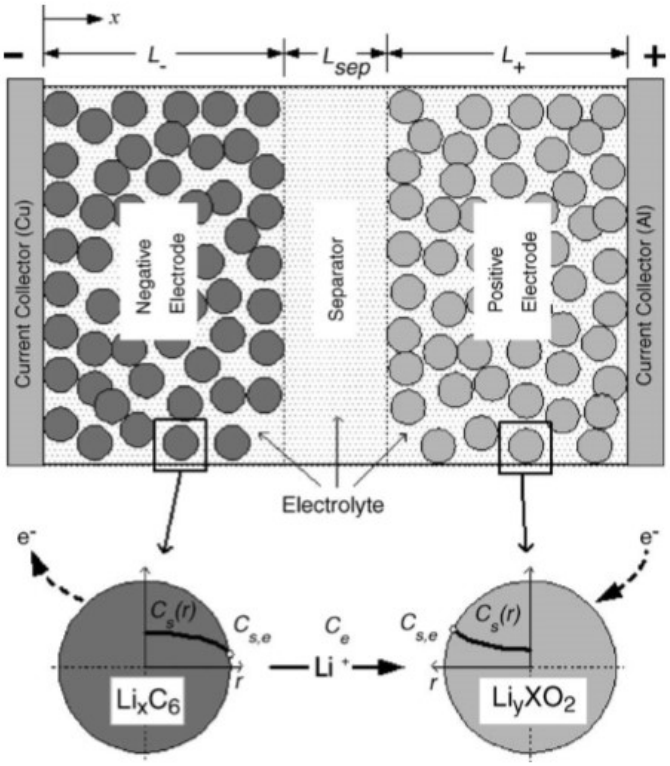

Figure 6: 1D representation of the electrochemical cell model in the x-direction and the 1D coupled solid diffusion model in the r-direction. [18]

The macroscopic model uses the concentrated solution theory, this theory accounts not only for the interactions of ions with the solvent but also between each other. The groundwork for the concentrated solution theory is Stefan-Maxwell multicomponent diffusion (see equation 1) where the interactions between the two species *i* and *j* in the electrolyte is represented by $\mathfrak{D}_{ij}$. In this formulation, $\nabla\mu_i$ stands for the gradient of the electrochemical potential, c_T is the total concentration of the species present in the electrolyte. The temperature in Kelvin is given by T and gas constant is given by R [17] [19].

$$c_i \nabla \mu_i = RT \sum_j \frac{c_i c_j}{c_T \mathfrak{D}_{ij}} \tag{1}$$

The model also uses the porous-electrode theory developed by Newman et al. The interface between the Different sections of the cell are assumed to be continuous in the model, so there is a connectivity between all nodes in the model. The active material particles are assumed to be spherical, furthermore, the change in volume during insertion and de-insertion is neglected. In addition, the diffusion coefficient of lithium in active material is assumed to be constant and independent of concentration. The electrolyte is treated as binary (single salt and single solvent), even for cases where a mixture of solvents is used [18] [21].

Following the theories of porous electrode and concentrated solution, one can obtain equation 2 which presents a conservation equation for the salt/ions in the electrolyte phase. The porosity is represented with ε, which is the void volume fraction where the electrolyte can reside. The concentration is a function of both time (*t*) and space (*x*). The effective diffusion coefficient is given by D and the specific interfacial area a which describes the surface area of the pore walls per unit volume of the total electrode. The rate of species transfer between the solid phase and the electrolyte is represented by j_{+n} and is set to zero in the separator. There are two types of currents inside the cell: the ionic current given by $i_{2,x}$ which is relevant along the whole cell (electrodes and separator) and the electrical current which is only valid in the electrode sections [10].

$$\varepsilon\frac{\partial c}{\partial t} = \frac{\partial}{\partial x}\left(D\left(1-\frac{dlnc_0}{dlnc}\right)\frac{\partial c}{\partial x}\right) + (1-t_+^0)aj_{+n} - \frac{i_{2,x}}{F}\frac{\partial t_+^0}{\partial x} \tag{2}$$

The potential (φ_2) in the electrolyte phase is formulated as equation 3. The activity coefficient is expressed as f_A. The equations 2 and 3 are the only relevant equations for the separator in the model [17].

$$\frac{\partial \varphi_2}{\partial x} = -\frac{i_{2,x}}{\kappa_{eff}} + \frac{RT}{F}\left(1+\frac{\partial lnf_A}{\partial lnc}\right)(1-t_+^0)\frac{\partial lnc}{\partial x} \tag{3}$$

Equation 4 correlates the pore-wall flux of lithium, at the solid phase interface with the electrolyte phase, to the divergence of ionic current [17].

$$aj_{+n} = \frac{1}{F}\frac{\partial i_{2,x}}{\partial x} \tag{4}$$

Equation 5 models the kinetics of (de)insertion reaction for the active materials using the Butler-Volmer equation. The exchange current density is given by $i_{0,x}$. The anodic and cathodic transfer coefficients expressed as $\alpha_{2,a}$ and $\alpha_{2,c}$, respectively. The overpotential is represented by $\eta_{s,2}$ and is equal to $\varphi_1 - \varphi_2 - U$, U is the equilibrium potential of the insertion process or in other words the OCP of the active materials [17].

$$j_{+n} = \frac{i_{0,x}}{F}\left[exp\left(\frac{\alpha_{2,a}F\eta_{s,2}}{RT}\right) - exp\left(\frac{\alpha_{2,c}F\eta_{s,2}}{RT}\right)\right] \tag{5}$$

The potential in the solid phase of the electrode is described with the Ohm's law. In equation 6, the electronic current $i_{1,x}$ has been replaced with the total current I minus the ionic current ($i_{2,x}$).

$$\frac{\partial \varphi_1}{\partial x} = -\frac{I - i_{2,x}}{\sigma_{eff}} \tag{6}$$

Finally, the conservation of lithium (c_s) in the active material is described with equation 7

$$\frac{\partial c_s}{\partial t} = D_s \left(\frac{\partial^2 c_s}{\partial r^2} + \frac{2}{r} \frac{\partial c_s}{\partial x} \right) \tag{7}$$

The equation 2-7 are then used to simulate a full-cell LIBs, those six equations are coupled equations with six dependent unknown variables(c, φ_2, c_s, $i_{2,x}$, j_{+n}, φ_1). For the half-cell, equations 6 and 3 can be combined into one equation (see equation 8). There are only five dependent unknown variables for the half-cell configuration (c, η, c_s, $i_{2,x}$, j_{+n}) [17].

$$\frac{\partial \eta}{\partial x} = -\frac{I}{\sigma_{eff}} + i_{2,x} \left(\frac{1}{\sigma_{eff}} + \frac{1}{\kappa_{eff}} \right) - \frac{RT}{F} \left(1 + \frac{\partial ln f_A}{\partial ln c} \right) (1 - t_+^0) \frac{\partial ln c}{\partial x} \tag{8}$$

Doyle numerically solved the abovementioned system of equations during his Ph.D. thesis with the use of Newman's Band algorithm. In this method, equations are discretized using the central difference approach and control volume for the boundaries [17] [4].

The simulation of LIBs is a very complex numerical problem. Moreover, there are many possible combinations of electrodes materials with different properties. Here, Doyle's simulation program was used. This program was originally written in Fortran and has been used in this project as a base to simulate LIBs. Researching and experimenting with various cathode materials gives a better understanding of the performance of LIBs. In future it is even possible to expand the program to simulate the multi-layer electrodes.

4 Program

4.1 Graphical user interface

The Doyle program is purely text-based and can be difficult to operate with when is not familiar with programming languages and/or battery theory. Therefore a graphical user interface (GUI) was developed. The GUI was designed to help the user simulate a battery with relative ease. The main window consists of four sections, shown in Figure 7, which will be explained briefly. The GUI is written in C/C++ and uses Doyle's Fortran simulation program as a library.

First, the user must decide to simulate a half-cell or a full-cell battery. The window will change accordingly, changing its layout slightly, adding or removing an anode material selection menu. Next section is devoted to the electrode and separator. When half-cell is selected, most of the menus in the anode sections is disabled because a lithium foil is the only appropriate material. This is done to prevent mistakes and to avoid irrelevant simulations. Then in the 'Simulation options' section, there is a possibility to adjust various data from temperature to print options. Last, there is an option to save and/or load the simulation settings where the user can load parameters or save the settings of the current simulation. This saves time especially when simulating the same battery over and over to match the experimental data.

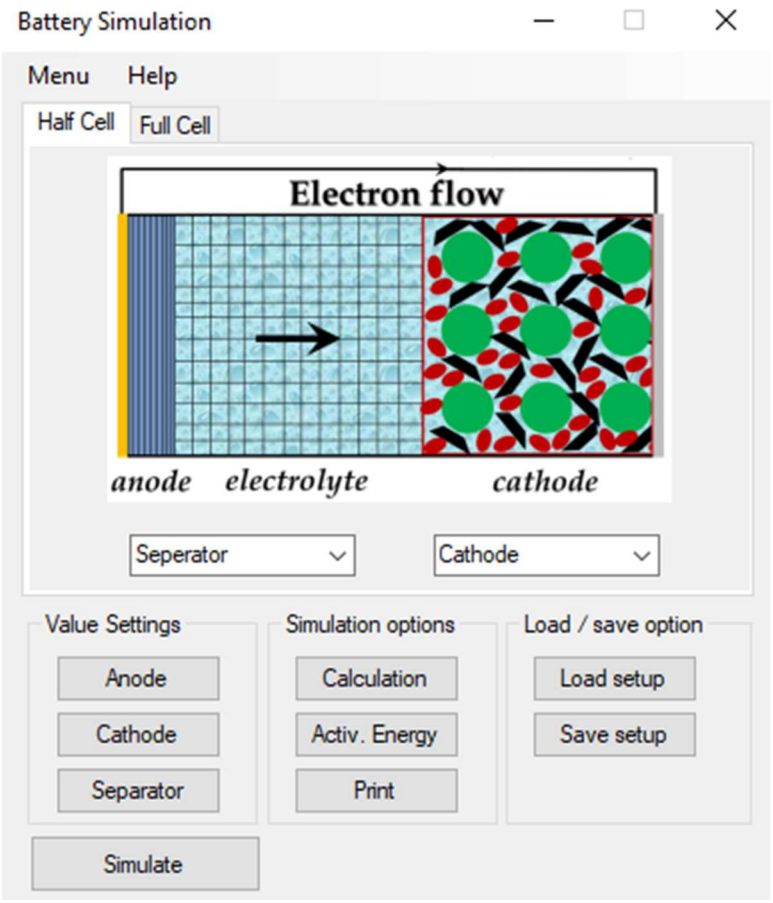

Figure 7: The main window

Figure 8 shows the 'Anode settings' window, where the user has to provide input for the anode when simulating a full-cell battery. The text fields show what dimensions should be entered, making it more user-friendly and to avoid mistakes. Before the GUI accepts the entered data, the values will be analyzed. Every field must be filled, and only numerical values can be used. The GUI accepts scientific notations, like the E-notation. The decimal point is used as a separator, meaning a comma will not be recognized as a separator. When the data does not fulfill the criteria a warning message is generated, explaining what is wrong.

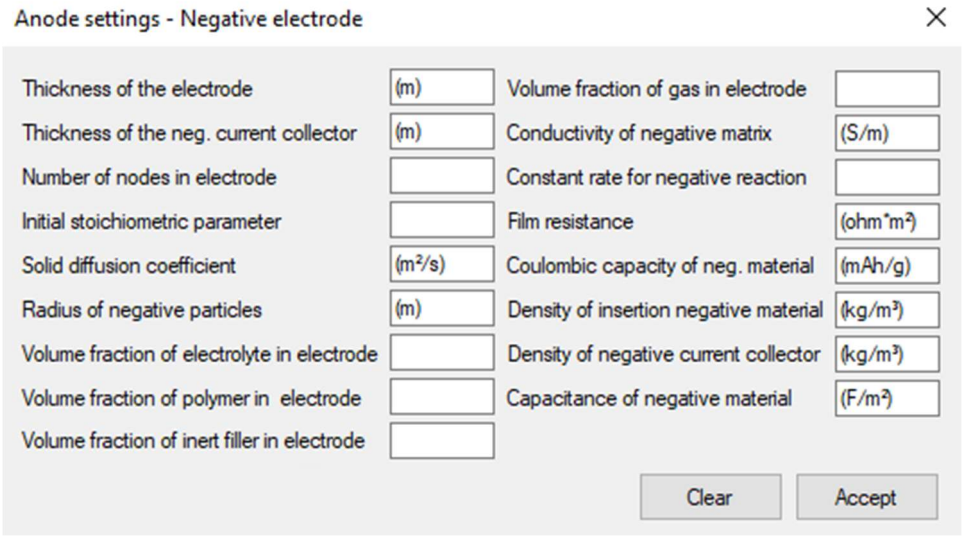

Figure 8: Negative electrode settings

Under 'Calculation', it is possible to define an arbitrary load profile (e.g., charge or discharge) using a timetable, shown in Figure 9. Here, the order of charge, discharge, or relaxation (i.e., no load) together with the load values and termination conditions (e.g., cut-off voltage or time). The charge and discharge modes will be explained later in more detail. Figure 9 shows an example of a schedule where first, the battery will discharge to a cutoff potential of 3V using 18 A/m^2 in galvanostatic mode. The battery will then rest for one hour before charging at 15 A/m^2 in potentiostatic mode with a cutoff voltage of 4.2 V.

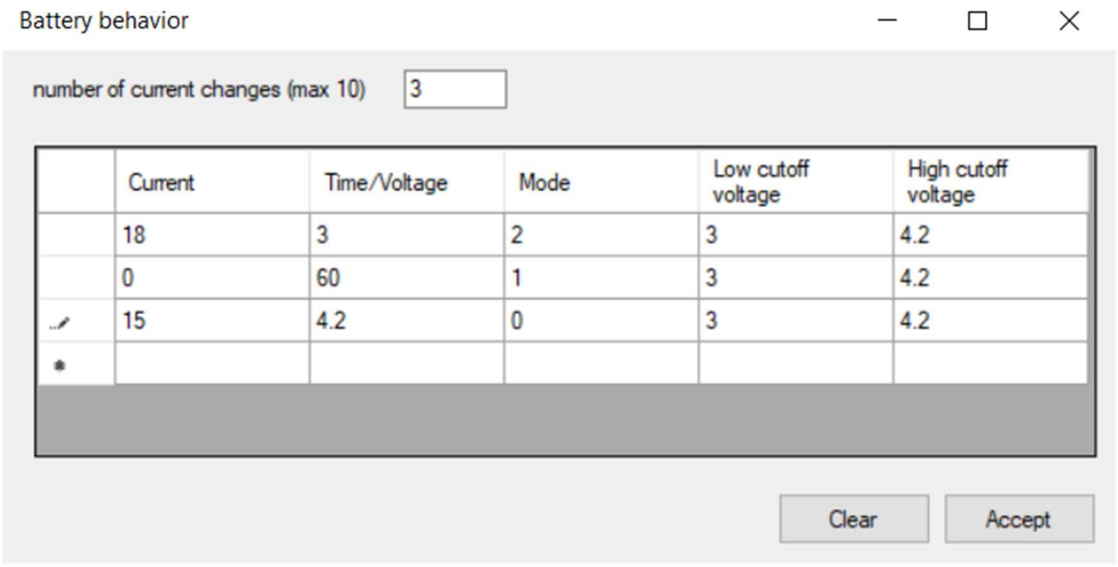

Figure 9: Charge/discharge scheduler

4.2 Description of the Dualfoil program

To give a better understanding of how the simulation program works, there will be a brief description of the most important functions. Figure 10 shows a flowchart of the program. Different colors and shapes are used, each with its own meaning. Various shapes represent functions or predefined processes. The yellow square represents a single function whereas the purple rectangle represents a collection of functions. The different processes will be explained in more detail. The red diamonds are for user-specified decisions, according to these decisions the calculation method will slightly change. Last, the blue rectangles show a loop, i.e., the program will continue or stop if a condition is met. Some functions are more difficult than others, therefore a small flowchart will be used to illustrate how they work.

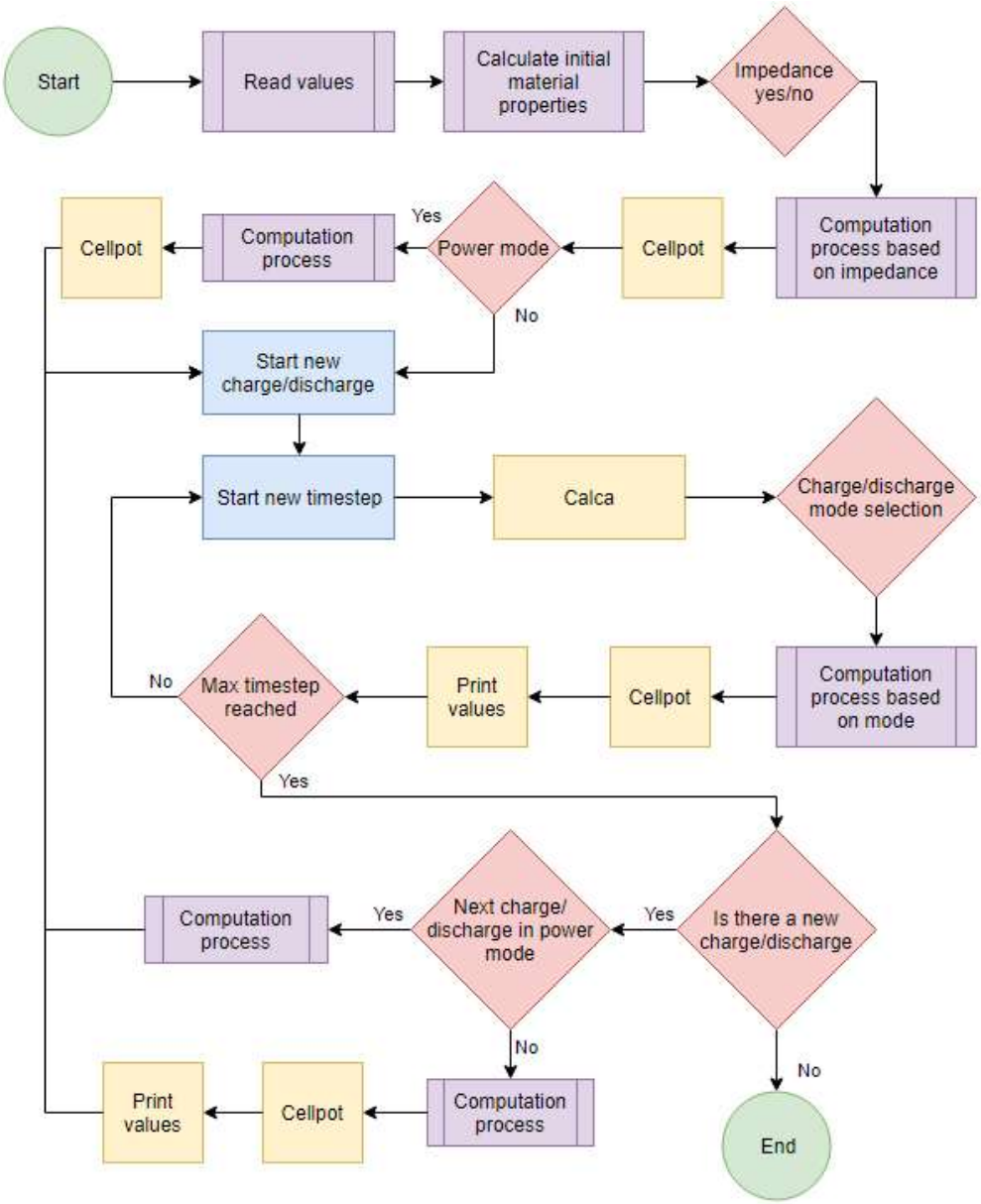

Figure 10: Flowchart of the Dualfoil program

First, the program will receive data from the graphical user interface (GUI). After receiving data from the GUI, the program starts to initiate. This means that it starts to calculate important values and converting other values to the necessary format and inserting them in the right arrays.

Some important examples of initial data calculation and conversion:

- calculation of specific particle area in each electrode

$$a = \frac{particle\ shape(1-\varepsilon)}{R_S} \tag{9}$$

  There are three possible particle shapes: planar, cylindrical and spherical. Each using the following numbers: 1, 2, 3.

- calculation of total concentration in the active material (AM)

$$\mathrm{ct} = \frac{3600 * specific\ capacity * density\ of\ AM}{F} \tag{10}$$

Next, the calculation of initial material properties. Here the function EKIN, PROP and MASS gets called. The function EKIN generates the Butler-Volmer kinetic expression for an electrode, there are two electrodes so this function will be called two times. After that, the function PROP gets called, which passes on the correct transport properties of the chosen electrolyte. Last, the function MASS gets called. Here the mass of the battery is calculated in kg/m2 based on densities and volume fractions of the components.

Based on the user input the execution will slightly change. For example, when there is no impedance the function COMP is called on. The function COMP is the main calculation function of this program. It will process all the equations of the battery model. In every single run, the unknowns are solved for the entire thickness of the battery, X=0 to X=L. When there is impedance the function COMP is called upon multiple times resulting in different values. This is an example of a predefined process in the flowchart. These kinds of decisions and processes will happen a lot throughout the program.

Note that the initial phase of the program is not finished. To initiate the calculation of the first time step there needs to be an initial cell potential which is calculated in the function CELLPOT. At this point, all the initial values to start the simulation are known.

The user has the option to choose the charge/discharge mode to simulate the battery's behavior. There are two important charge/discharge techniques, galvanostatic and potentiostatic. These techniques are used to examine the behavior of the cathode and the anode by polarizing the electrodes in the electrolyte.

First, the galvanostatic method is used for determining the electrochemical reaction rate by applying a constant current to an electrode and observing the change in the voltage of the electrode as a function of time [20]. The second method is the potentiostatic technique, here a constant potential is applied instead of a constant current and the time evolution of the current is recorded [21].

There are six different ways the program can simulate the charge and discharge of the battery:

- Potentiostatic charge/discharge
- Galvanostatic charge/discharge for a given time
- Galvanostatic charge/discharge to a cutoff potential
- Galvanostatic charge/discharge for a given time with taper mode (i.e., constant voltage)
- Charge/discharge using a specified power (in W/m2)
- Charge/discharge using a specified load (in ohm-m2)

Based on the selected technique, the program will start the simulation. In every time step, the diffusion of phenomena in the active material particles should be calculated which is done in the function CALCA. After each time step, an output files will be generated. This print includes information such as time, potential, heat generated, resistance, concentration, etc.

As shown in Figure 10, the program will keep calculation until a stopping condition is satisfied. This can be a specified time or a specified cutoff potential. The program also stops simulating when there is an error in the function COMP. This might happen, for instance, when there is no enough lithium in the cathode or when the battery has reached a negative potential.

After the simulation is done, the GUI will show potential over time graph. All the output files are generated in the map 'output'. The program generates six different files:

- General: the user's input and basic output like weight, energy and power of the cell
- Half cell: output values in the case of a half-cell simulation
- Output: output values based on user's choices
- Resistance: the resistance throughout the cell
- Solid-state concentration profiles: information about the concentration of lithium in the AM
- Concentration profiles in electrolyte: information about change of concentration of the electrolyte, etc.

4.2.1 Comp

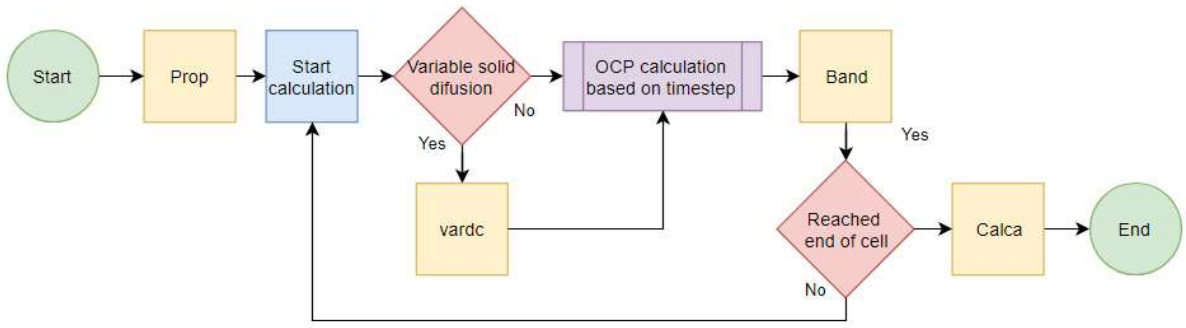

Figure 11: Flowchart of the comp subroutine

Figure 11 shows the flowchart of COMP, this is the main computational function of the program. This function is going through the equations of the cell 'sandwich', meaning it is going to solve the sets of six or seven equations, previously mentioned, simultaneously at each time step.

The user has the option to choose the number of nodes per section of the battery. A node can be seen as a one-dimensional position in the battery. For example; the length of a cathode with hundred nodes is divided into hundred equal segments. The entire thickness of the battery is the sum of the nodes of all the three segments (anode, cathode, and separator). Every time COMP runs, it will iterate the sum of the nodes. More node ensures a more accurate simulation but with a longer computation time.

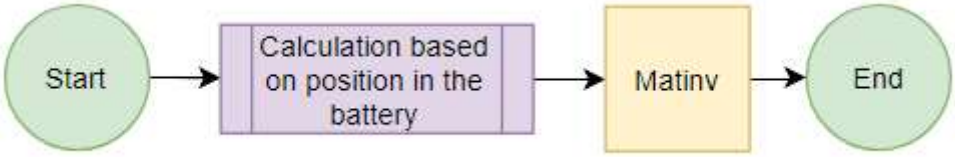

Figure 12: Flowchart of the BAND subroutine

Before COMP starts, it calls the PROP. This will provide the transport properties of the electrolyte. Then four arrays are initialized, these arrays will contain the values the subroutine BAND will use in each iteration. BAND is a solver for a system of coupled linear differential equation and is a very important part of the program because there are six or seven dependent unknown variables that need to be solved simultaneously in every time step.

As mentioned before Newman's BAND is a solver for one dimensional coupled linear differential equations. Figure 12 shows the flowchart of BAND, it uses a tridiagonal matrix structure and can solve a system of n equations with j intermediate point. Boundaries are needed for j=1 and j=nj positions in order to solve the equations. For the internal boundaries one can use the control volume method [4] or alternatives for BAND such as MBAND [22] and the extension of Newman's numerical technique [23]. A matrix inversion function checks for errors and will report if an error is detected.

In the next step, the function starts to calculate the 'sandwich'. There is an option to simulate the variable solid state diffusion coefficient. When this option is enabled an extra function is called upon which is not used in this thesis. It is also possible to include the side reactions in the simulations, which add more complexity to the calculation.

In every iteration, EKIN is called to renew the Butler-Volmer kinetic expressions. When every equation has been run through and every value is in the right array, BAND will solve for the unknown variables. When the final node in the x direction is reached, CALCA will calculate the diffusion process and COMP ends. Otherwise, a new iteration will start.

4.2.2 Ekin

This subroutine produces the Butler-Volmer kinetics expression for the anode and cathode when simulating a full-cell battery and only for the cathode when simulating a half-cell battery. This expression illustrates the mathematical relation between the overpotential ($E - E_{eq}$) and the current density of an electrode.

$$j = j_0 \left[\exp\left(\frac{\alpha_a z F \eta}{RT}\right) - \exp\left(-\frac{\alpha_c z F \eta}{RT}\right) \right] \tag{11}$$

with,

$$\eta = E - E_{eq} \tag{12}$$

The expressions are generated based on the open-circuit potential (OCP) of the chosen active material for each electrode. The function provides a library of OCPs for different active materials. It is possible to add new OCPs to the function. However, the OCPs have to be in a functional form in terms of the solid state concentration and the first derivative with respect to the concentration is also needed as an input before the program can use them.

Below are the OCPs of LMO [17], NMC [24], LCO [25] and LFP [26] which are used in this thesis. In equations 13 to 16, y stands for the state of charge (SOC).

$$\begin{aligned} U_{LMO}(y) = {} & 4.19829 + 0.0565661 \tanh(-14.5546y + 8.60942) \\ & - 0.0275479 \left(\frac{1}{(0.998432 - y)^{0.492465}} - 1.90111 \right) \\ & - 0.157123 \exp(-0.04738 y^8) \\ & + 0.810239 \exp\big(-40(y - 0.133875)\big) \end{aligned} \tag{13}$$

$$\begin{aligned} U_{NMC}(y) = {} & 6.51176 - 8y + 7.1086y^2 - 1.55y^3 - 0.459y^6 \\ & - 5.00034 \times 10^{-8} \exp(135.089y^2 - 118.089), \end{aligned} \tag{14}$$

$$\begin{aligned} U_{LCO}(y) = {} & 3.855 + 1.247(1 - y) - 11.152(1 - y)^2 \\ & + 42.818(1 - y)^3 - 67.710(1 - y)^4 \\ & + 42.508(1 - y)^5 - (6.132e - 04) \exp\left(7.657(y^{115})\right) \end{aligned} \tag{15}$$

$$U_{LFP}(y) = 3.135 - 0.685(-ln(y)0.478 - 1.342y + 1.734e^{0.4(y-1)} \tag{16}$$

4.2.3 Prop

The transport properties of various electrolytes are stored in PROP. This subroutine is a library for different electrolytes. Like EKIN, it is possible to add values to create a custom binary electrolyte.

Below is a list of parameters the user is able to enter:

- Diffusion coefficient of the salt
- First derivative of diffusion coefficient with respect to the electrolyte concentration
- Conductivity of the salt
- First derivative of the conductivity of the salt with respect to the electrolyte concentration
- Transference number
- First derivative of transference number with respect to the electrolyte concentration
- Activity factor for salt
- Derivative of activity factor for salt with respect to the electrolyte concentration

4.2.4 Mass

Here the mass of the battery is calculated based on the densities and volume fractions of the different components. The mass per unit area of the battery is in kg/m², it includes one electrode and separator for half-cell and two electrodes and separator for the full-cell, together with the current collectors.

Half-cell formula

$$Mass = \delta_s \left[\rho_s\left(1-\varepsilon_e\varepsilon_p\right)_s + \rho_e\varepsilon_e + \rho_p\varepsilon_p\right] + \delta_+ \left[\rho_+\left(1-\varepsilon_e\varepsilon_p\varepsilon_f\right)_+ + \rho_e\varepsilon_e + \rho_p\varepsilon_p + \rho_f\varepsilon_f\right] + \delta_{-cc}\rho_{-cc} + \delta_{+cc}\rho_{+c} \quad (17)$$

Full-cell formula

$$Mass = \delta_- \left[\rho_-\left(1-\varepsilon_e\varepsilon_p\varepsilon_f\right)_- + \rho_e\varepsilon_e + \rho_p\varepsilon_p + \rho_f\varepsilon_f\right] + \delta_s \left[\rho_s\left(1-\varepsilon_e\varepsilon_p\right)_s + \rho_e\varepsilon_e + \rho_p\varepsilon_p\right] + \delta_+ \left[\rho_+\left(1-\varepsilon_e\varepsilon_p\varepsilon_f\right)_+ + \rho_e\varepsilon_e + \rho_p\varepsilon_p + \rho_f\varepsilon_f\right] + \delta_{-cc}\rho_{-c} + \delta_{+c}\ \rho_{+cc} \quad (18)$$

4.2.5 Sol

The solid-phase concentration profiles are calculated in this subroutine. A separate file is created where the values are stored. The file contains the concentration of lithium in the particles of an electrode. A profile is generated at each time step and for all the nodes.

4.2.6 Calca

The diffusion process is an important step in the simulation. Here the diffusion of lithium in the solid particles of the active material is calculated. This function takes into account that there are three possible shapes of particles and that they each can have different sizes. When simulating a half-cell battery, the calculation of the Lithium diffusion in the anode is skipped because there is no diffusion in the foil. Using the r-direction of the particle as the direction normal to the surface gives a material balance for lithium

$$\frac{\delta c_s}{\delta t} = \frac{\delta^2 c_s}{\delta r^2} + \frac{2}{r}\frac{\delta c_s}{\delta r} \tag{19}$$

The following two boundary conditions are used,

$$\frac{\delta c_s}{\delta r} = 0 \; at \; r = 0 \tag{20}$$

and

$$J_n = -D_s \frac{\delta c_s}{\delta r} \; at \; r = R_s. \tag{21}$$

These equations can be solved by using a superposition integral, since D_s is considered to be constant, making it a linear problem.

4.2.7 Cellpot

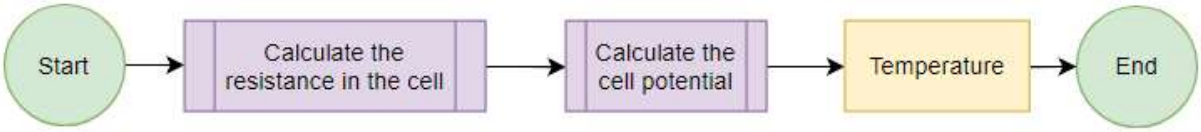

Figure 13: Flowchart of the cellpot subroutine

Here the potential of the cell is calculated together with the cell's resistance and its temperature. The function generates a file where it will print some values for that specific timestep. The function will run one time per timestep. The values that are printed:

- Time
- Utilization of electrode material
- Cell potential
- OCP potential
- Current load
- Temperature
- Heat generation

The cell's potential is calculated by the difference in solid-phase potential of the two electrodes (x=0 and x= $\delta_- + \delta_s + \delta_+$). Before the resistance is calculated, EKIN is called to refresh the kinetic expressions. This is done to take into account for the changes after each time step, then the resistance is calculated using Ohm's law. The resistance is calculated for cathode, anode, and separator. Last, the sum of these values is taken as the total resistance of the cell for a given time step.

5 Results & Discussion

5.1 Verification of the Dualfoil program

Since the Dualfoil program has been revised during the years it was important to verify the simulation results with some reference simulations. To do so, we compared our simulation results with those reported in the thesis of Doyle from 1995 for a graphite/LMO cell using the same input parameters. Figure 14 compares the results of our simulation (left side) with those of Doyle's (right side). There is a good agreement between the two groups of simulations especially for 0.1C, 0.5C, and 1C. However, when looking at the higher c-rates, there is a small difference in voltage drop. These small differences can be explained by the fact that we didn't have access to all of the parameters and some had to be found using trial and error.

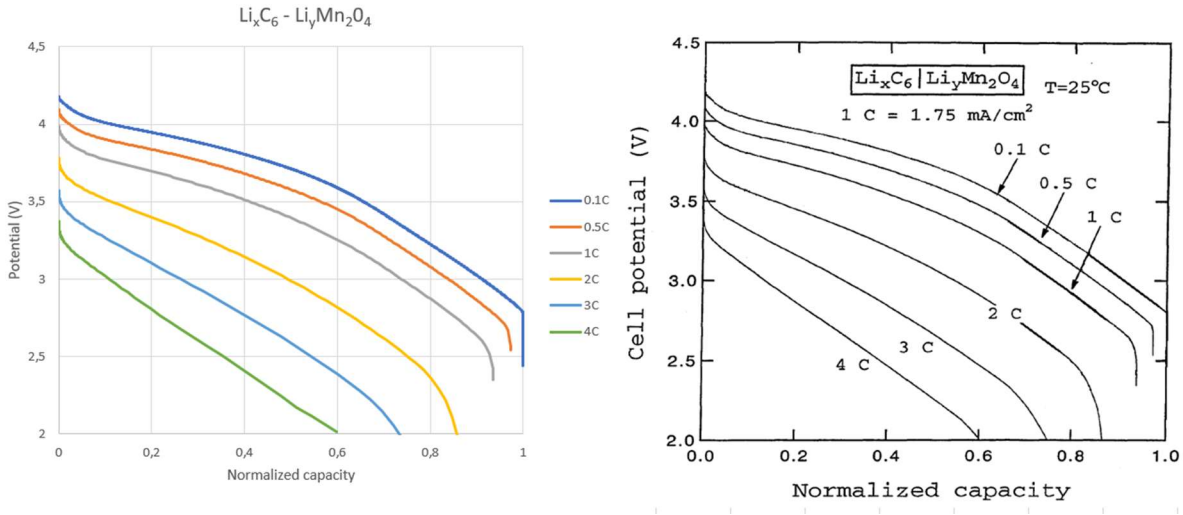

Figure 14: Comparison of the revised Dualfoil program (2018) and the program from Doyle's thesis (1995).

5.2 Base case simulation properties

The initial parameters used in the simulation of NMC, LMO, LCO, and LFP can be seen at Table 4. The parameters of NMC are taken from Smekens et al [27]. To determine the parameters of the other materials trial and error is used to reach the practical capacity from literature of each material.

Table 4: Initial parameters of NMC, LMO, LCO and LFP

Electrode	**NMC**	**LMO**	**LFP**	**LCO**
Density active material	4770 kg/m^3	4140 kg/m^3	3600 kg/m^3	5010 kg/m^3
Density carbon/additive	1800 kg/m^3			
Density current collector	2707 kg/m^3			
Density current collector	8954 kg/m^3			
Diffusion coefficient	3.04e-14 m^2/s	3.7e-14 m^2/s	1.8e-14 m^2/s	3.9e-14 m^2/s
Electric conductivity	3.8 S/m			
Ionic conductivity	1.36 S/m			
Particle radius	1.72e-6 m	8.5e-6 m	1.0e-6 m	4.0e-6 m
Porosity	44%	40%	50%	40%
Reaction rate constant	4.38e-11	2.0e-11	2.0e-11	1.0e-11
Thickness current collector	25.0e06 m			
Thickness electrode	46.0e06 m	50.0e-6 m	50.0e-6 m	50.0e-6 m
Volume fraction carbon/additive	6.8%	6.5%	4.76%	7.66%
State of charge (SOC)	0.42	0.18	0.01	0.437
Separator				
Density electrolyte	1324 kg/m^3			
Initial salt concentration	1000 mol/m^3			
Porosity	40%	50%	50%	40%
Thickness separator	20.0e-6 m	25.0e-6 m	25.0e-6 m	25.0e-6 m

5.3 Sensitivity analysis

Here, the sensitivity of the discharge performance of NMC, LMO, LCO, and LFP in half-cells to different design parameters is analyzed. The studied parameters are: thickness, %active material in cathode, diffusion coefficient, electronic and ionic conductivity of the cathode, and electrode porosity. First, we discuss the expected results according to the available literature. Second, we present and discuss our results. Finally, we compare our simulation results with the literature. The seven parameters and their range used in the sensitivity analysis are summarized in table 5. Some materials did not reach their cut-off voltage at certain parameters values, this will be also discussed.

Table 5: Parameters used during sensitivity analysis

Parameters	**Values range**
Cathode thickness	25 – 50 – 75 – 100 – 125 – 150 – 175 (μm)
Active material wt%	80 – 85 – 90 – 95 (%)
Diffusion coefficient	e-13 – e-14 – e-15 – e-16 (m^2/s)
Electronic conductivity	0.1 – 1 – 10 – 100 (S/m)
Ionic conductivity	0.1 – 1 – 10 – 100 (S/m)
Porosity	0.3 – 0.4 – 0.5 – 0.6

5.3.1 C-rates and area under the curve (AUC)

The current with which a LIB is (dis)charged is often expressed in C-rates (see equation 22). If a battery is fully (dis)charged in *n* hours then its C-rate is reported 1/n. The discharge curve is plotted with respect to the specific capacity (mAh/g). One can derive from the discharge or charge curve if the LIB is working according to its specifications.

$$C-rate = \frac{current\ (discharge\ or\ charge)}{electrical\ charge\ capacity\ of\ the\ cell, module, battery} = \frac{1}{drain\ time\ (h)} \quad (22)$$

To verify if the four cathode materials are achieving their specific capacity, discharge graphs are shown. The LCO cathode material has a practical capacity around 140 mAh/g at 1 C-rate. The capacity will decrease at higher C-rates which is a general trend independent of the active material. The NMC cathode material has a practical capacity between 160-170 mAh/g, for the LMO cathode material the practical capacity is around 120 mAh/g, and for the LFP cathode material this is between 150-160 mAh/g. The maximum load current the cell can deliver is determined at the point when the electrode is delivering less than 70% of its capacity, this depends on how well the cell is been made [28].

The specific capacity shown in Figure 15 is from the cathode active material, not from the total cathode. The total mass of the cathode includes the mass of the active material, the mass of the electrolyte, and mass of the binder and additive. Therefore, the capacity of the total cathode will be smaller than the capacity of the cathode material. The specific capacity is close to the practical capacities that the LIBs should have. The specific capacity of a material depends highly on Li-ion diffusivity and the electrical conductivity. Layered materials like LCO and NMC have a superior Li-ion diffusivity and electrical conductivity over LFP and LMO, as result LCO and NMC have a higher specific capacity [12].

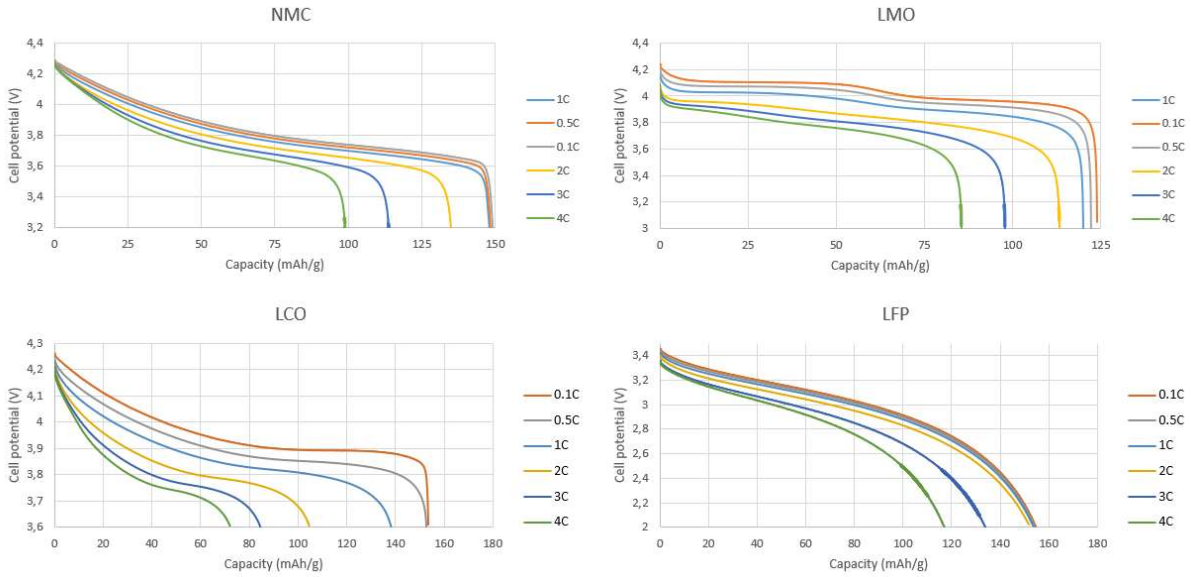

Figure 15: Discharge curve of NMC, LMO, LCO and LFP

The drop in the voltage during discharge at higher c-rates is a result of higher polarization which is caused by a variety of resistances inside the cell: ionic resistance, electronic resistance, and the interfacial resistance. The electrode particles and the electrolyte contribute to the ionic resistance. For the electrical resistance, the electrode particles, conductive additives, percolation network of additives in the electrode, current collectors and the electrical taps are contributing. The interfacial resistance is the resistance occurring at the border between electrolyte and electrodes, between electrode particles and conductive particles, between the electrode and the current collector and between the conductive additive and the current collector [12]. The shape of the discharge curve is primary determined by the chosen OCV function.

The specific energies (Wh/kg) for NMC, LMO, LCO, and LFP are shown in Figure 16. The specific energy is easily explained as the area under the discharge curve. The lower the C-rates, the higher the area under the discharge curve which gives a higher specific energy. Going higher in C-rates will result in lower specific energy. The specific energy for the NMC and the LCO have almost an equal trend in the drop in energy at higher c-rates, note that energy loss for the LCO is higher which is a disadvantage for the LCO compared to NMC. The high rate performance of LFP compared to other materials can be confirmed in this figure. The same should be said about LMO but the performance is not on the same level as LFP. It is noteworthy that our simulation does not account for the unique features of the LFP electrode, i.e., two-phase (de)insertion and resistive reactant. This explains why the shape of discharge curves for LFP are not representatives of the reality where a two-phase plateau is present at intermediate SOCs.

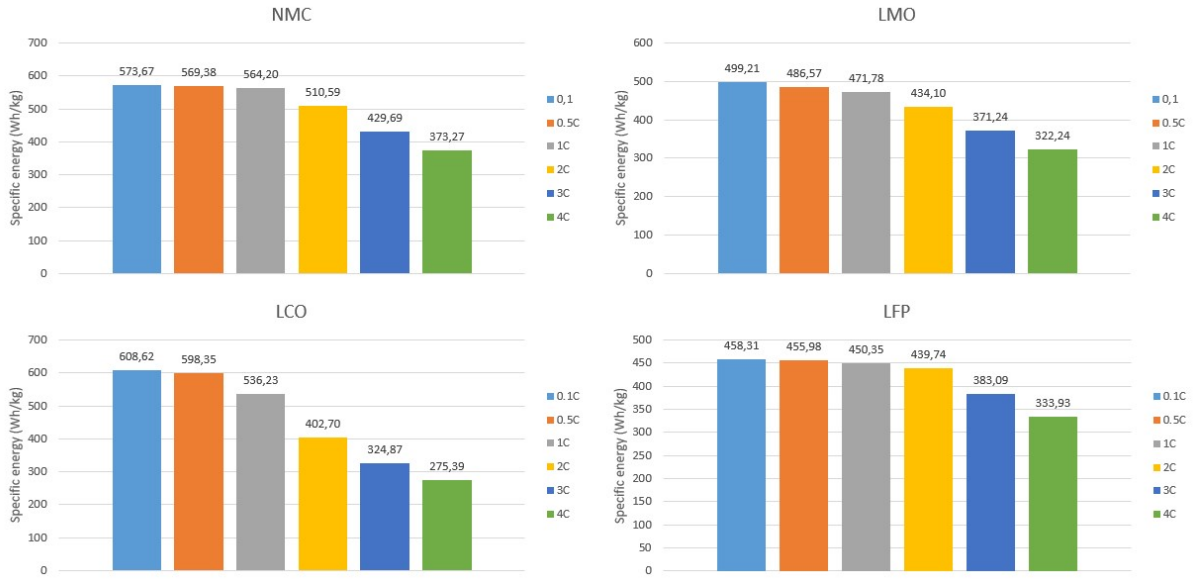

Figure 16: Specific energy of NMC, LMO, LCO and LFP at 1 c-rate

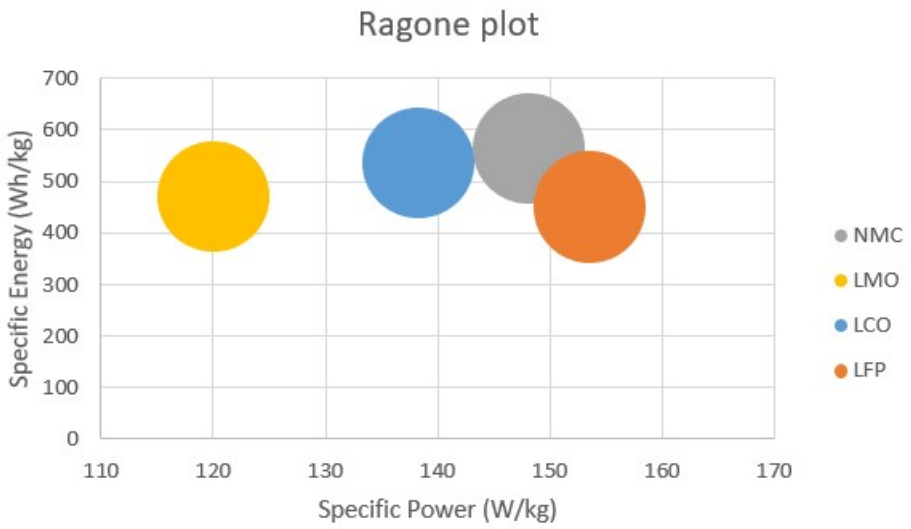

Figure 17: Ragone plot of NMC, LMO, LCO and LFP at 1 c-rate

In Figure 17, the Ragone plot is presented for LCO, LFP, NMC, and LMO. This plot is used to compare the performances of the four cathode materials. The Ragone plot shows the specific energy (Wh/kg) versus the specific power (W/kg). We see that LMO has a high specific energy but a low specific power, LCO has a moderate specific energy and specific power, LFP can deliver a high specific power but has a relatively low specific energy, NMC has a high specific power with a relatively higher specific energy.

5.3.2 Thickness

The electrode thickness has a big impact on the specific energy and the power of a cell. According to a study on thickness analysis by Zheng et al. [28] . By increasing the thickness, the specific energy will increase and the specific power will decrease. Furthermore, thinner electrodes maintain a higher capacity at high c-rates while thicker electrodes have a decrease in capacity at high c-rates. However, regardless of the thickness, the cell can deliver almost its full capacity at low c-rates of 0.1 or lower. The decrease in the capacity for thicker electrodes is due to the higher internal resistance

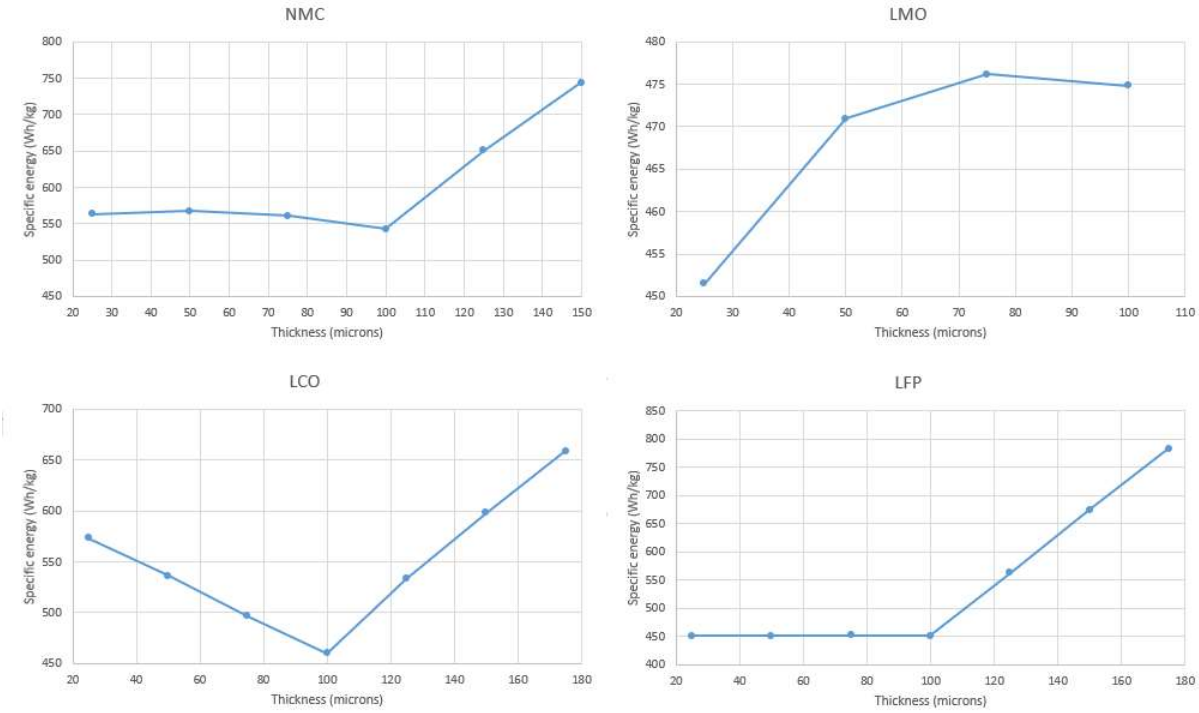

Figure 18: Thickness analysis; specific energy of NMC, LMO, LCO and LFP at C-rates where the cell reaches its cut-off potential

Figure 18 shows the variation of specific energy as a function of cathode thickness. Specific energy slightly decreases for NMC and LFP up to a thickness of 100 microns. A similar trend is observed for LCO but with a larger decrease. In the case of LMO, energy reaches its maximum at a thickness around 75 microns. The discharge simulations did not reach the cut off voltages for thicknesses above 100 and 150 microns for LMO and NMC, respectively.

Figure 19 presents the sensitivity of the specific power to the thickness of the electrodes. All four cathodes experience a decrease in specific power which is expected for thicker electrodes.

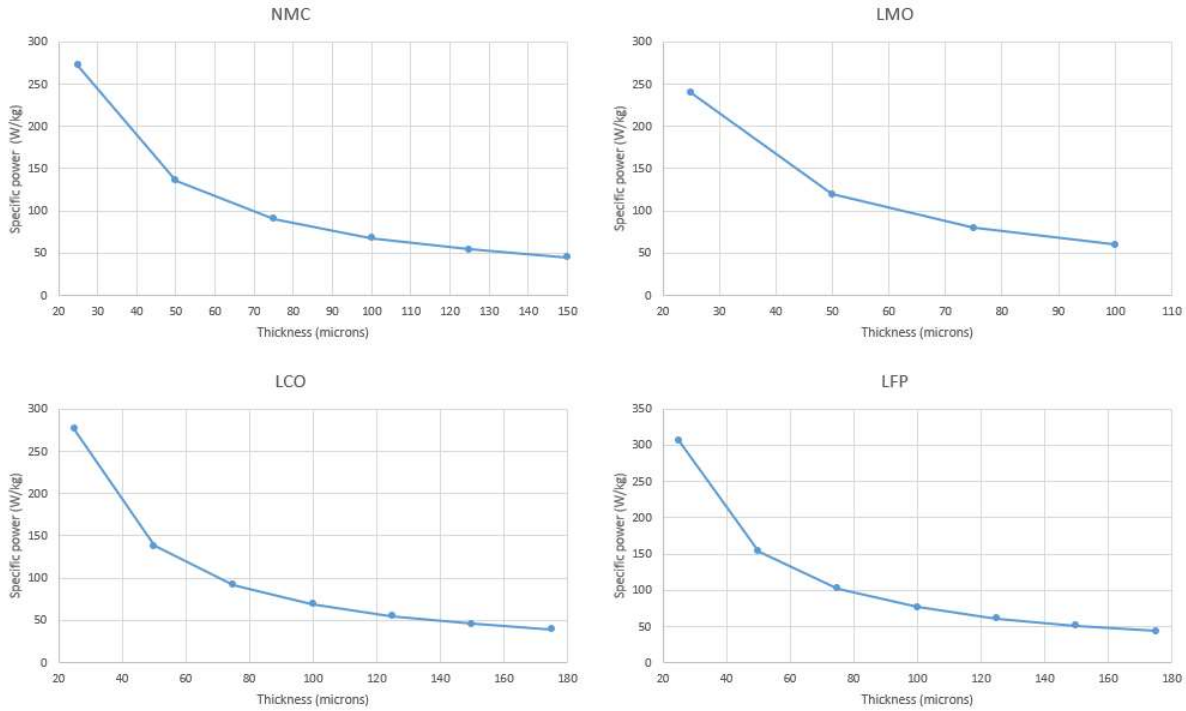

Figure 19: Thickness analysis; specific power of NMC, LMO, LCO and LFP at C-rates where the cell reaches its cut-off potential

Our simulations indicate that the salt concentration is driven to zero when exceeding thickness of 100 microns and 125 microns for LMO and NMC, respectively. As a result, there will be a premature end of discharge.

One of the challenges in thick electrodes is the transport limitations in the electrolyte. This was verified by performing similar simulations for the thickness effect but using higher values of diffusion coefficient of Li salt in the electrolyte. So it is essential to select an electrolyte with a high enough diffusion coefficient for thick electrodes.

5.3.3 Active material percentage

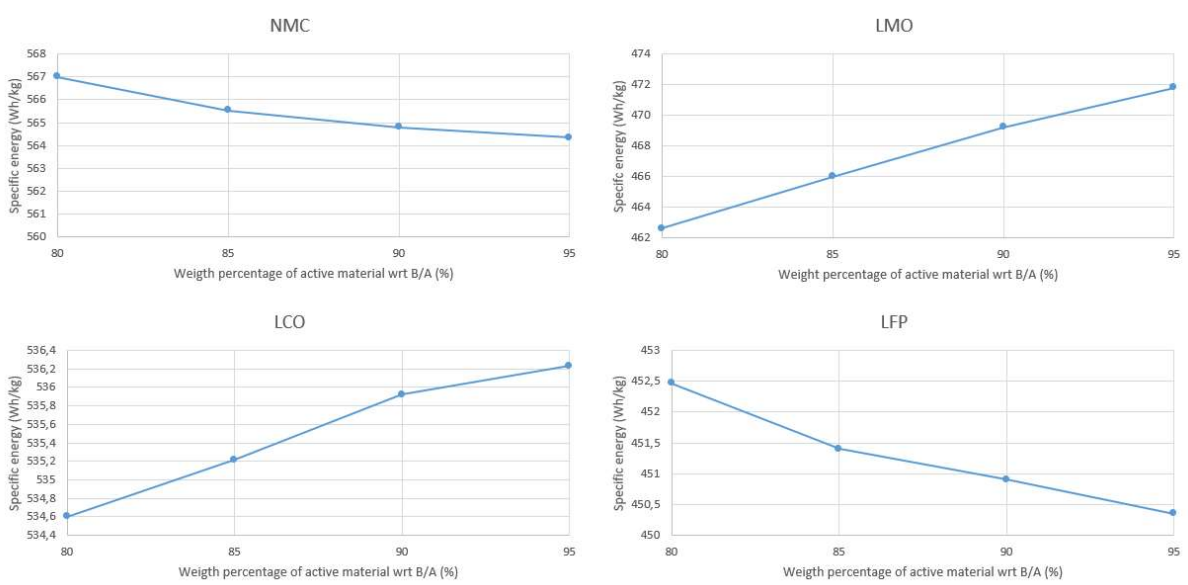

Figure 20: AM% analysis wrt B/A; specific energy of NMC, LMO, LCO and LFP at C-rates where the cell reaches its cut-off potential

Increasing the AM percentage with respect to the binder and the additive will result in the decline of the specific power of the cell for all four materials. Different situations might happen for the specific energy when increasing the ratio of the active-material of an electrode while using the same thickness. For example, a decrease in the specific energy at higher active-material fraction might be expected given the relatively high values of density in transition-metal oxide electrodes against additive and binder. On the other hand, a rise in the transport limitations inside the electrolyte as a result of lower porosity can decrease the capacity and hence the specific energy of the cell. Figure 20 shows a monotonous increase in the specific energy of LCO and LMO when the Wt% of active material increases whereas an opposite trend is observed for LFP and NMC.

5.3.4 Solid diffusion coefficient

Diffusion is a process which produces a net flow of matter from an area of high concentration or chemical potential to an area of low concentration or chemical potential. The diffusing species possess a chemical potential, the difference in the quantity of chemical potential over a distance is what drives the diffusion process. Some of the most important parameters of a Li-ion battery is determined by the diffusion process, these parameters include charge and discharge rate, capacity and cycling stability [12].

It is hard to measure the solid state diffusivity or diffusion coefficients. The diffusivity is approximated from the total conduction which is the sum of electrical conduction and ionic conduction. Active material structures affects the diffusion coefficient [12]. There are three commercialized structures discussed in this paper, shown in Figure 21.

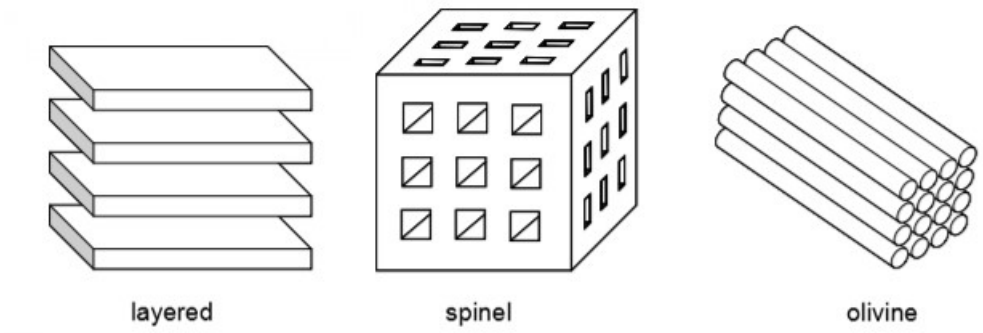

Figure 21: Simple representation of the 2D layered, 3D spinel and 1D olivine structure, obtained from [29]

First, both NMC and LCO have a 2D layered structure where the flow of solid particles can diffuse in two dimensions. Second, LMO has a spinel structure which is a 3d structure, the diffusivity is 3 dimensional. Finally, LFP has a 1D structure where diffusivity is only possible in one direction [12].

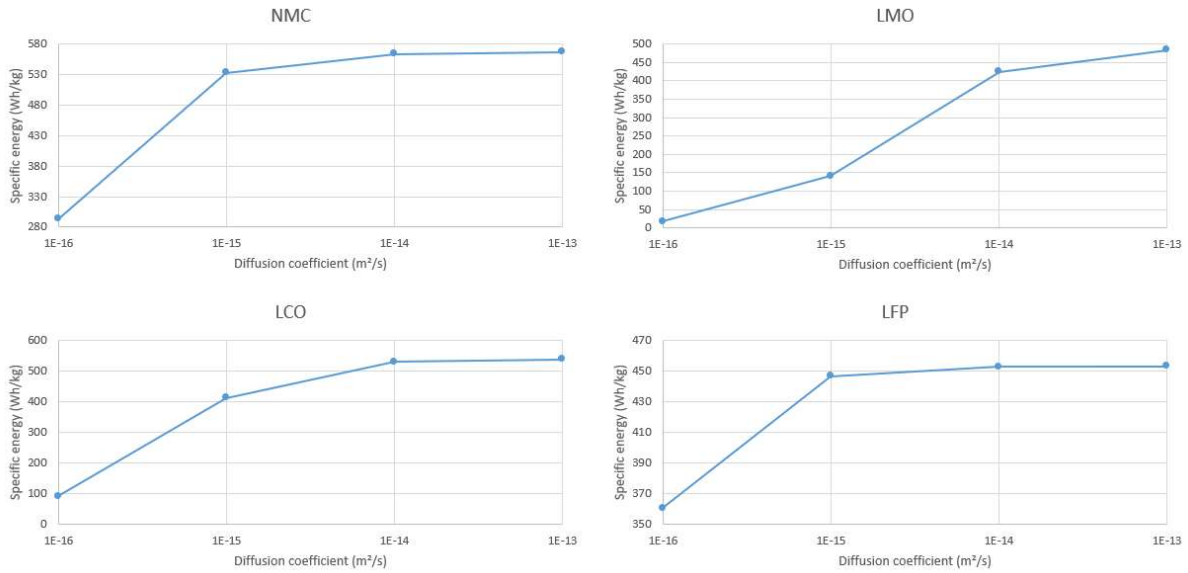

Figure 22: Solid diffusion coefficient analysis; specific energy of NMC, LMO, LCO and LFP at 1 C-rate

The effect of Li diffusivity on the specific energy is presented in Figure 22. Higher values of diffusion coefficient for Li inside the active material increase the specific energy of the cell. A high sensitivity to the diffusion coefficient up to 1e-14 m^2/s is seen for the four cathodes. Further increase of the specific energy above 1e-14 is insignificant for NMC, LCO, and LFP.

5.3.5 Electronic conductivity

Increasing the electronic conductivity of the electrode at a fixed thickness will result in a decrease in the cell ohmic resistance and therefore a better high c-rate performance. The electronic conductivity is an intrinsic property of the materials used in the formulation of the electrode.

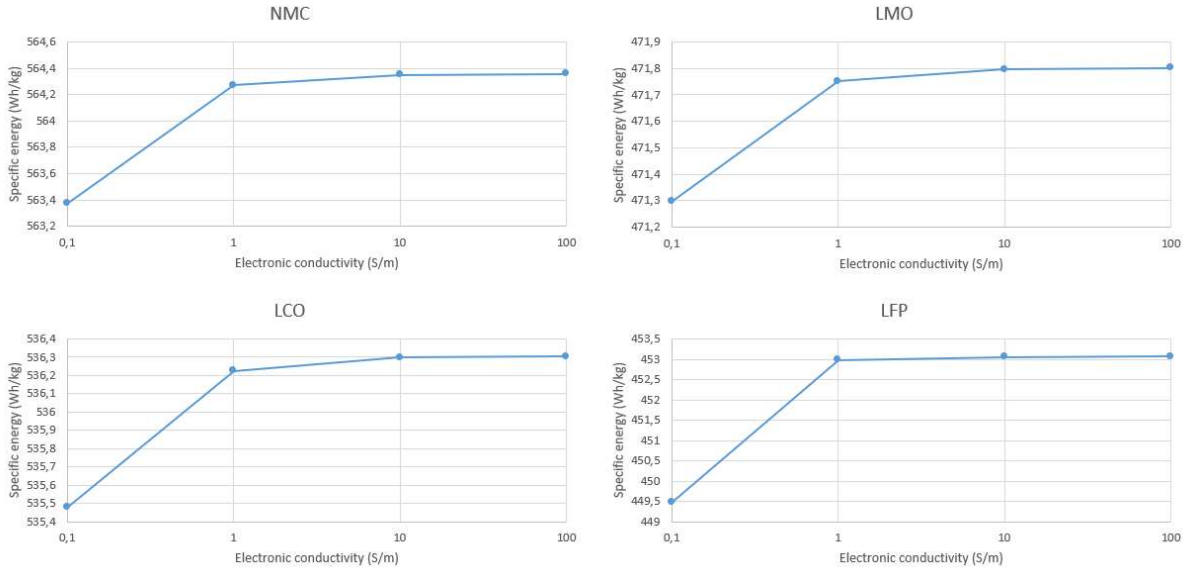

Figure 23: Electronic conductivity analysis; specific energy of NMC, LMO, LCO and LFP at 1 C-rate

Figure 23 shows the effect of electronic conductivity on the specific energy. According to Doyle [17], the lower the electronic conductivity goes, how steeper the discharge curve decreases to the cut-off voltage, which gives less area under the curve and results in less specific energy. The steep decrease is due to increased resistance. At higher electronic conductivity, the discharge curve will be closer to the shape of the OCV curve of the material. Going higher than 1 S/m, there is a negligible change in the specific energy.

5.3.6 Ionic conductivity

Ionic conductivity is one of the transport properties of the electrolyte. Ionic conductivity is important for understanding the motion of Li-ions. Anything that decreases the mobility of ions inside the electrolyte will result in a reduction of the ionic conductivity [12].

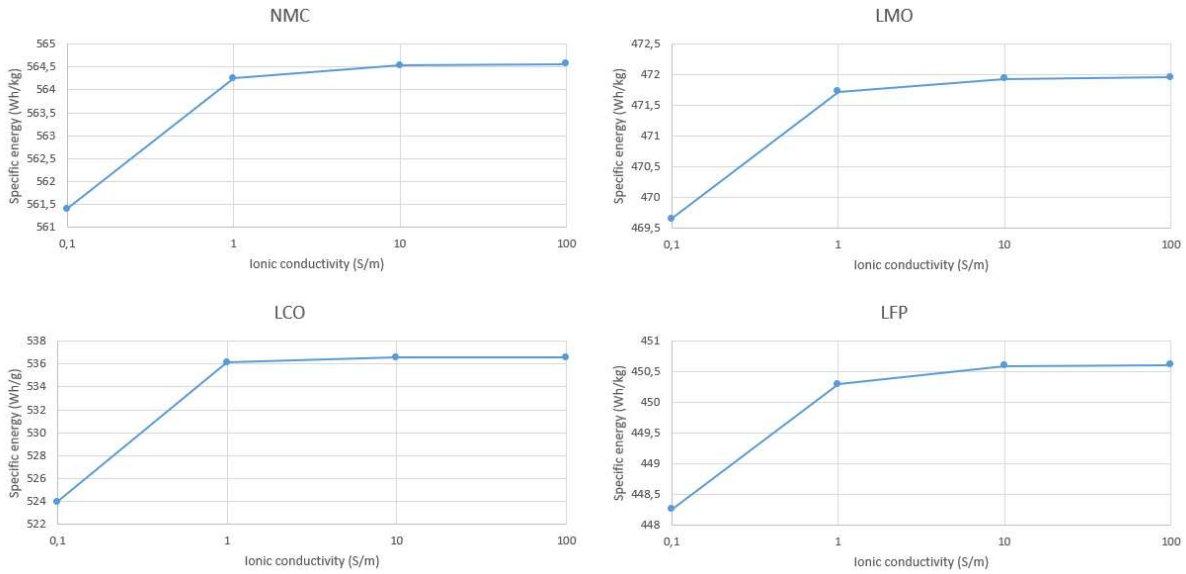

Figure 24: Ionic conductivity analysis; specific energy of NMC, LMO, LCO and LFP at 1 C-rate

Higher values of ionic conductivity will result in a higher specific energy, as result of the reduction of the cell polarization, similar to the case of electronic conductivity. This can be seen in Figure 24. There is a significant increase at first, after a certain point the increase is less. The same things said for the electronic conduction can be said for the ionic conduction. The only difference is that the ionic conductivity depends on the electrolyte formulation whereas the electronic conductivity depends on the properties of the porous electrode.

5.3.7 Porosity

The flux of electrolyte through a porous medium depends on many factors of which the porosity and tortuosity are the very important ones. The porosity is the space between the particles where the electrolyte can flow. The tortuosity is a complex microstructure property of the porous medium and is a measure of the complexity of an open path between two points. So there is a clear relation between those two. Increasing the porosity will give the electrolyte more place to move, and result in a decrease in tortuosity, and when decreasing the porosity it leads to an opposite effect [30].

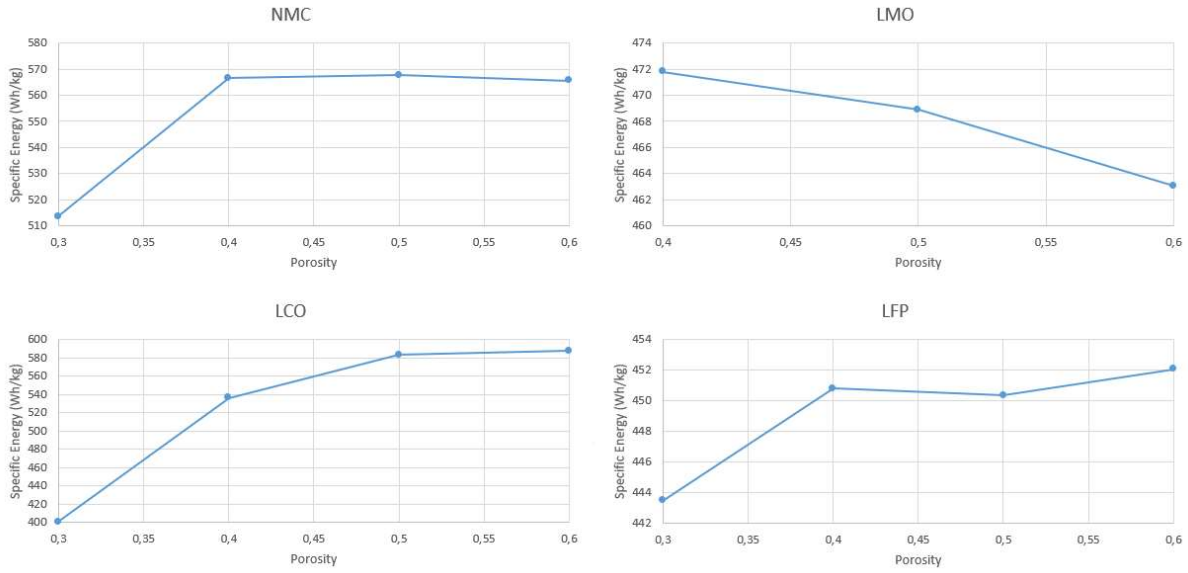

Figure 25: Porosity analysis, specific energy of NMC, LMO, LCO and LFP at C-rates where the cell reaches its cut-off potential

Increasing the porosity will reduce the weight of the active material and of the total electrode. At a fixed electrode thickness the increase in porosity means the reduction in volume for the active material as well for the binder and additives. The weight of the active material and binder and additive are replaced with the weight of the electrolyte which has a lower density compared to the active material. Figure 25 shows that when the porosity is 0.3 the specific energy is lower compared to higher porosity for the NMC, LCO and LFP materials. As mentioned before tortuosity is the main contributor for the decrease in specific energy. A similar trend is observed for NMC, LMO, and LFP where the specific energy first increases for the porosities up to 0.4-0.5 and then levels off at higher porosities. Specific energy of LMO, however, decreases for LMO when the porosity increases from 0.4 to 0.6. Figure 26 shows that at larger porosities the specific power increases for all the studied cathodes.

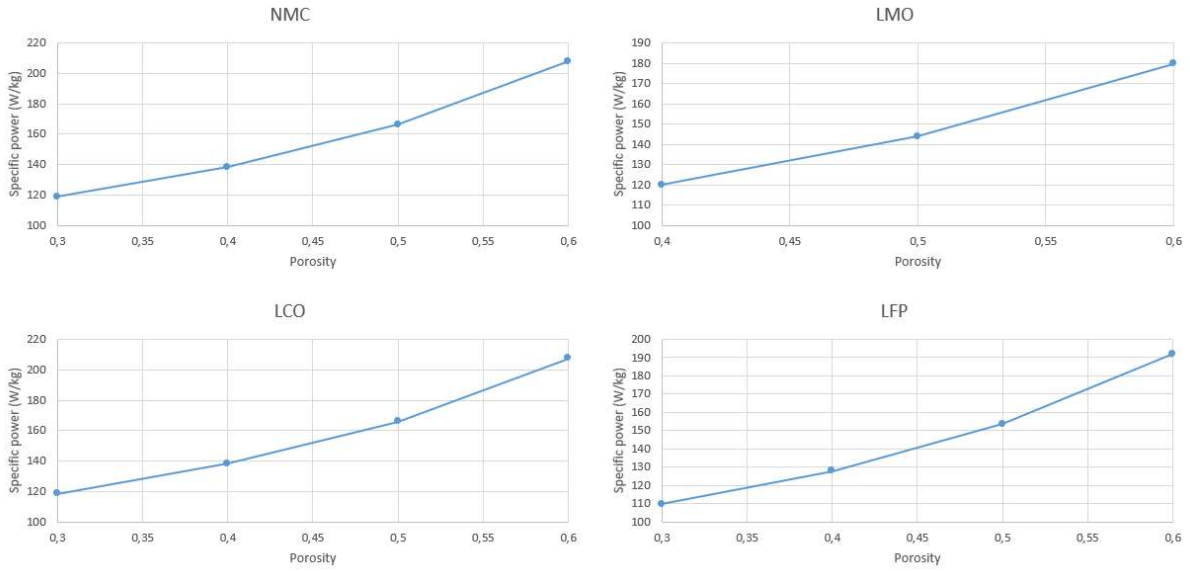

Figure 26: Porosity analysis; specific power of NMC, LMO, LCO and LFP at C-rates where the cell reaches its cut-off potential

6 Conclusion

The sensitivity of the half-cell performance to the design parameters was studied for NMC, LMO, LCO and LFP cathodes with the help of physics-based simulation (Dualfoil program). To summarize, the increase in the thickness of the cathode leads to an increase in the specific energy and a reduction in the specific power. For thicker electrodes and at high c-rates, a premature end-of-discharge might happen due to the lithium depletion in the electrolyte. In such cases, the application of an electrolyte formulation with better transport properties is essential. The increase of the weight percentage of the active material with respect to the binder and conductive additives results in the reduction of the specific power and the specific energy. The specific energy increases at higher values of solid state diffusion coefficient. The increase of electronic and ionic conductivity will reduce the overall cell resistance and increases the specific energy of the cell. As for the porosity, larger porosity will reduce the tortuosity which increases the specific energy. However, increasing the porosity above a certain point will reduce the specific energy due to the lack of enough active material inside the electrode. To conclude, the performance of a battery is sensitive to many parameters. Here, modeling and simulation proves to be a powerful tool to reduce the complexity and save time in finding the optimum set of parameters to reach the specific needs of the user.

7 Bibliography

[1] IMEC, "IMEC (Interuniversity Micro-Elektronics Centre)," IMEC, [Online]. Available: https://www.imec-int.com. [Accessed 16 10 2017].

[2] Uhasselt, "University of Hasselt," [Online]. Available: https://www.uhasselt.be/UH/IMO/About-IMO-IMOMEC. [Accessed 16 10 2017].

[3] Uhasselt, "University of Hasselt," EMAP, [Online]. Available: https://www.uhasselt.be/UH/IMO/Visit-the-groups/Engineering-materials-amp-amp-applications-(EMAP).html. [Accessed 16 10 2017].

[4] J. Newman and K. E. Thomas-Alyen, Electrochemical Systems, Berkeley: A John Wiley & Sons, INC Publication, 2004.

[5] J. Newman, "cchem.berkeley.edu," 1998. [Online]. Available: http://www.cchem.berkeley.edu/jsngrp/dualfoil5.2.f. [Accessed 1 05 2018].

[6] A. Yoshino, "The Birth of the Lithium-Ion Battery," *Angewandte Chemie International Edition,* vol. 51, pp. 5798-5800, 2012.

[7] B. Scrosati, J. Hassoun and Y.-K. Sun, "Energy & Environmental Science; Lithium-Ion batteries. A look into the future," *The Royal Society of Chemistry,* vol. 4, pp. 3287-3295, 2011.

[8] V. Srinivasan, "Batteries for vehicular applications.," in *AIP conference proceedings physics of sustainable energy*, Lawrence Berkeley, 2008.

[9] M. Safari, "Fundamentals of Battery Engineering," University Hasselt Diepenbeek, 2017.

[10] J. Newman and W. Tiedeman, "Porous-Electrode Theory with Battery Applications," *AlChe Journal,* no. Vol. 21, No. 1, pp. 25-38, 1975.

[11] A. Dushina, "Electrochemical Study of the Electrolytes/ Active Material Interaction in Aqueous Metal-Ion Batteries," Ruhr-Unversity Bochum, Bochum, 2016.

[12] M. Park, X. Zhang, M. Chung, G. B. Less and M. A. Sastry, "A review of conduction phenomena in Li-ion batteries," *Journal of Power Sources,* no. 195, pp. 7904-7929, 2010.

[13] C. M. Julien, A. Mauger, K. Zaghib and H. Groult, "Comparative Issues of Cathode Materials for Li-Ion Batteries," *inorganicas,* no. 2, pp. 132-1254, 2014.

[14] N. Nitta, F. Wu, J. T. Lee and G. Yushin, "Li-ion battery materials: present and future," Elsevier Ltd., Atlanta, Changsa, 2014.

[15] M. M. Doeff, "Battery cathodes," in *Encyclopedia of Sustainability Science and Thechnology*, University of California, Berkeley, Springer, 2013, pp. 4614-5791.

[16] L. O. Valoen and J. N. Reimers, "Transport Properties of LiPF6-Based Li-ion Battery Electrolytes," *Journal of the Electrochemical Society,* no. 152, pp. 882-891, 2005.

[17] C. Doyle, Design and Simulation of Lithium Rechargeable Batteries, vol. Development of Model Equations, Berkeley: Lawrence Berkeley National Laboratory, August 1995, p. 22.

[18] K. Smith and C.-Y. Wang, "Solid-state diffusion limitations on pulse operations of a lithium ion cell for hybrid electric vehicles," *Journal of Power Sources,* vol. 2006, no. 161, pp. 628-639, 2006.

[19] H. Abdul-Zehra, "Fuel Cells and Batteries," University of Babylon.

[20] "Corrosionpedia," [Online]. Available: https://www.corrosionpedia.com/definition/575/galvanostatic. [Accessed 1 8 2018].

[21] "Corrosionpedia," [Online]. Available: https://www.corrosionpedia.com/definition/915/potentiostatic. [Accessed 1 8 2018].

[22] D. Fan and R. E. White, "Modification of Newman's BAND(j) Subroutine to Multi-Region Systems Containing Interior Boundaries: MBAND," *Journal of the Electrochemical Society,* pp. 1688-1691, 1991.

[23] J. Van Zee, G. Kleine, R. E. White and J. Newman, "Extension of Newman's Numerical Technique to pentadiagonal systems of equations," in *Electrochemical cell design*, New York, Plenum Press, 1984, pp. 377-389.

[24] Z. Mao, M. Farkhondeh, M. Pritzker, M. Fowler and Z. Chen, "Multi-Particle Model for z Commercial Blended Lithium-Ion Electrode," *Journal of the Electrochemical Society ,* vol. 163, no. 3, pp. A458-A469, 2016.

[25] M. Doyle and Y. Fuentes, "Computer Simulations of a Lithium-ion Polymer Battery and implications for Higher Capacity Next-Generation Battery Designs," *Journal of the Electrochemical Society,* no. 6, pp. A706-A713, 2003.

[26] C. e. Zhang, "A Generalized SOC-OCV Model for Lithium-IOn Batteries and the SOC Estimation for LNMCO Battery," *energies,* vol. 9, no. 900, 2016.

[27] J. Smeken and et al, "A modified multiphysics model for lithium-ion batteries with a LixNi1/3Mn1/3Co1/3O2 electrode," *Electrochimica acta,* no. 174, pp. 615-624, 2015.

[28] H. Zheng, J. Li, X. Song, G. Liu and V. S. Battaglia, "A comprehensive understanding of electrode thickness effects on electrochemical performances of li-ion battery cathodes," *Electrochimica Acta,* vol. 265, no. 71, p. 258, 2012.

[29] West-Virginia University, "web.statler.wvu.edu," [Online]. Available: https://web.statler.wvu.edu/~wu/mae493/7-storage-2.pdf. [Accessed 1 08 2018].

[30] M. Matyka, A. Khalili and Z. Koza, "Tortuosity-porosity relation in the porous media flow," *Physical Review E,* vol. 2008, 2008.

[31] D. Linden and T. B. Reddy, Handbook of Batteries -3rd Editiion, T.R.D: McGraw-Hill, 2002.

[32] S.-T. Myung, Y. Hitoshi and Y.-K. Sun, "Electrochemical behavior and passivation of current collectors in lithium-ion batteries," *Journal of Materials Chemistry,* no. 21, pp. 9891-9911, 2011.

[33] F. La Mantia, "Characteriwation of electrodes for lithium-ion batteries through electrochemical impedance spectroscopy and mass spectrometry," ETH Zurih, Zurih, 2008.

[34] M. Doyle and J. Newman, "The use of mathematical modeling in the design of lithium/polymer battery systems," *Electrochemica Acta,* no. 40, pp. 2191-2196, 1995.

Auteursrechtelijke overeenkomst

Ik/wij verlenen het wereldwijde auteursrecht voor de ingediende eindverhandeling:
Model-based optimization of electrodes for lithium-ion batteries

Richting: **master in de industriële wetenschappen: elektronica-ICT**
Jaar: **2018**

in alle mogelijke mediaformaten, - bestaande en in de toekomst te ontwikkelen - , aan de Universiteit Hasselt.

Niet tegenstaand deze toekenning van het auteursrecht aan de Universiteit Hasselt behoud ik als auteur het recht om de eindverhandeling, - in zijn geheel of gedeeltelijk -, vrij te reproduceren, (her)publiceren of distribueren zonder de toelating te moeten verkrijgen van de Universiteit Hasselt.

Ik bevestig dat de eindverhandeling mijn origineel werk is, en dat ik het recht heb om de rechten te verlenen die in deze overeenkomst worden beschreven. Ik verklaar tevens dat de eindverhandeling, naar mijn weten, het auteursrecht van anderen niet overtreedt.

Ik verklaar tevens dat ik voor het materiaal in de eindverhandeling dat beschermd wordt door het auteursrecht, de nodige toelatingen heb verkregen zodat ik deze ook aan de Universiteit Hasselt kan overdragen en dat dit duidelijk in de tekst en inhoud van de eindverhandeling werd genotificeerd.

Universiteit Hasselt zal mij als auteur(s) van de eindverhandeling identificeren en zal geen wijzigingen aanbrengen aan de eindverhandeling, uitgezonderd deze toegelaten door deze overeenkomst.

Voor akkoord,

Avci, Ferhat **Voets, Devlin**

Datum: **20/08/2018**